Reprinted from JOURNAL OF NEUROLOGY, NEUROSURGERY AND PSYCHIATRY, May 2007, Vol 78, p 548-549

Guillain–Barré syndrome with antibodies to GD1a/GD1b complex

Recently, ganglioside complexes (GSCs) such as GD1a/GD1b, GD1a/GM1, GD1b/GT1b, GM1/GT1b, GQ1b/GM1 and GQ1b/GD1a have been

shown as target antigens for serum antibodies in patients with Guillain–Barré syndrome (GBS)[1] and Miller Fisher syndrome (MFS).[2] Gangliosides may interact with each other to form a novel epitope, which serves as a target antigen for serum antibodies.[1] In paticular, anti-GD1a/GD1b IgG is reported to be associated with severe GBS and requirement of mechanical ventilation.[1] However, there has been no previous case report describing GBS with anti-GSC antibodies in detail. In this report, we present a patient with GBS having anti-GD1a/GD1b antibody and investigated the clinical feature.

Case report

A 42-year-old man noticed weakness of the bilateral upper extremities 2 weeks after an episode of acute respiratory tract symptoms and diarrhoea. His symptoms further developed to dysarthria, dysphagia and tetraparesis, and he was admitted to the Department of Neurology, Ishikawa Prefecture Central Hospital, Kanazawa, Japan, 4 days after the onset of weakness. Neurological examination disclosed bilateral facial weakness, poor elevation of the soft palate, hoarseness, dysarthria, dysphagia, weakness of the tongue, flaccid tetraparesis (grade 4, Medical Research Council scale) and areflexia of deep tendon reflexes. He needed a wheelchair for transfer, and stomach tube for gastrogavage. Laboratory findings including cerebrospinal fluid (CSF) examination were normal, except for hypercapnia (Pco_2 47.8 mm Hg) on blood gas analysis. Nerve conduction studies demonstrated a marked reduction of compound muscle action potentials (CMAP) with normal conduction velocity (CMAP was 2.87 mV and motor conduction velocity was 50.6 m/s in the right median nerve), but sensory nerves were normal. The MRI studies of the brain and spinal cord were normal. A diagnosis of GBS was made, and he was given intravenous immunoglobulin (IVIg; 400 mg/kg/day) and intravenous methylprednisolone (500 mg/day) for 5 days, according to the protocol used in the previously reported randomised trial.[3] He underwent rehabilitation, and his symptoms gradually improved 1 week after admission. He could stand by himself 2 weeks after admission, and eat by himself without a stomach tube 1 month after admission. Nerve conduction studies still showed simple reduction of CMAPs 1 month after admission (CMAP was 1.21 mV and motor conduction velocity was 53.0 m/s in the right median nerve). At 2 months after admission, he could ambulate independently. He returned to work (English teacher at a high school) 3 months after admission.

The antibodies to gangliosides (GM1, GM2, GM3, GD1a, GD1b, GD3, GT1b, GQ1b, GA1, Gal-C, and GalNac-GD1a) and GD1a/GD1b complex in the serum obtained on the first day of admission were examined by enzyme-linked immunosorbent assay, as previously described.[1 4] He was positive only to the antibody to GD1a/GD1b complex (anti-GD1a/GD1b antibody).

Comment

Our patient showed acute progressive axonal motor polyneuropathy involving the cranial nerves 2 weeks after flu-like symptoms. This condition fulfilled the established criteria of GBS, and the results of nerve conduction studies were classified as having acute motor axonal neuropathy (AMAN).[5] Anti-GD1a/GD1b antibody was detected in the acute-phase serum; however, there were no antibodies to single gangliosides, including GD1a and GD1b.

In a recent report,[1] 8 of 100 patients with GBS had anti-GD1a/GD1b antibodies, and three of these eight did not demonstrate any anti-ganglioside antibodies. These eight patients with anti-GD1a/GD1b antibody tended to have cranial nerve deficits and severe disabilities, and four of these patients required artificial ventilation.[1] Of the three anti-GD1a/GD1b antibody-positive patients with available electrophysiological data, two showed an axonal neuropathy pattern, and the remaining one showed an equivocal pattern.[1] Of the 12 patients with MFS, 7 had serum antibodies to some GSCs, and anti-GSC antibodies might influence the clinical features, as sensory signs were infrequent in patients with anti-GQ1b/GM1 antibody.[2] These findings may support the theory that anti-GSC antibodies correlate with a certain phenotype of GBS or MFS.

The clinical features of our patient were similar to those patients with anti-GD1a/GD1b antibodies,[1] such as AMAN-type GBS with cranial nerve deficits and severe disability (the Hughes Functional Grading Scale at the peak of his disability was on grade 4). Although our patient did not require artificial ventilation, his hypercapnia suggested respiratory weakness. The patient received intravenous methylpredonisolone in addition to IVIg. This combination therapy might prevent his case from being aggravated to grade 5. However, a future large-scale study will be needed to clarify this point.

Tsuyoshi Hamaguchi, Kenichi Sakajiri, Kenji Sakai, Soichi Okino
Department of Neurology, Ishikawa Prefecture Central Hospital, Kanazawa, Japan

Masami Sada, Susumu Kusunoki
Department of Neurology, Kinki University School of Medicine, Osaka-Sayama, Japan

Correspondence to: Dr T Hamaguchi, Department of Neurology, Ishikawa Prefecture Central Hospital, 2-1 Kuratsuki-higashi, Kanazawa 920-8530, Japan; gom56@ipch.jp

Informed consent was obtained for publication of the patient's details described in this report.

doi: 10.1136/jnnp.2006.108217

Competing interests: None declared.

References

1 **Kaida K**, Morita D, Kanzaki M, *et al.* Ganglioside complexes as new target antigens in Guillain–Barré syndrome. *Ann Neurol* 2004;**56**:567–71.
2 **Kaida K**, Kanzaki M, Morita D, *et al.* Anti-ganglioside complex antibodies in Miller Fisher syndrome. *J Neurol Neurosurg Psychiatry* 2006;**77**:1043–6.
3 **Van Koningsveld R**, Schmitz PIM, van der Meché, *et al.* Effect of methylprednisolone when added to standard treatment with intravenous immunoglobulin for Guillain–Barré syndrome: randomized trial. *Lancet* 2004;**363**:192–6.
4 **Kusunoki S**, Chiba A, Kon K, *et al.* N-acetylgalactosaminyl GD1a is a target molecule for serum antibody in Guillain–Barré syndrome. *Ann Neurol* 1994;**35**:570–6.
5 **Ho TW**, Mishu B, Li CY, *et al.* Guillain–Barré syndrome in northern China: relationship to Campylobacter jejuni infection and anti-ganglioside antibodies. *Brain* 1995;**118**:597–605.

Molecular Biology of the Cell
Vol. 18, 2112–2122, June 2007

Gangliosides GM1 and GM3 in the Living Cell Membrane Form Clusters Susceptible to Cholesterol Depletion and Chilling[D]

Akikazu Fujita,* Jinglei Cheng,* Minako Hirakawa,† Koichi Furukawa,‡ Susumu Kusunoki,† and Toyoshi Fujimoto*

Departments of *Anatomy and Molecular Cell Biology and ‡Biochemistry II, Nagoya University Graduate School of Medicine, Nagoya 466-8550, Japan; and †Department of Neurology, Kinki University School of Medicine, Osaka 589-8511, Japan

Submitted January 26, 2007; Revised March 6, 2007; Accepted March 20, 2007
Monitoring Editor: Jean Gruenberg

Presence of microdomains has been postulated in the cell membrane, but two-dimensional distribution of lipid molecules has been difficult to determine in the submicrometer scale. In the present paper, we examined the distribution of gangliosides GM1 and GM3, putative raft molecules in the cell membrane, by immunoelectron microscopy using quick-frozen and freeze-fractured specimens. This method physically immobilized molecules in situ and thus minimized the possibility of artifactual perturbation. By point pattern analysis of immunogold labeling, GM1 was shown to make clusters of <100 nm in diameter in normal mouse fibroblasts. GM1-null fibroblasts were not labeled, but developed a similar clustered pattern when GM1 was administered. On cholesterol depletion or chilling, the clustering of both endogenous and exogenously-loaded GM1 decreased significantly, but the distribution showed marked regional heterogeneity in the cells. GM3 also showed cholesterol-dependent clustering, and although clusters of GM1 and GM3 were found to occasionally coincide, these aggregates were separated in most cases, suggesting the presence of heterogeneous microdomains. The present method enabled to capture the molecular distribution of lipids in the cell membrane, and demonstrated that GM1 and GM3 form clusters that are susceptible to cholesterol depletion and chilling.

INTRODUCTION

Microdomains enriched with cholesterol and sphingolipids, or rafts, have been postulated to exist in the cell membrane (Simons and Ikonen, 1997). Domains showing a liquid-ordered state have been visualized in model membranes (Korlach *et al.*, 1999; Dietrich *et al.*, 2001a), but whether similar domains exist in the biological membranes of living cells, and what their basic properties would be, including size, life span and dynamics, are still under debate (Simons and Ikonen, 1997; Edidin, 2003; Munro, 2003; Kusumi *et al.*, 2004; Mayor and Rao, 2004; Mukherjee and Maxfield, 2004). Recent results, obtained by single-particle tracking and fluorescent resonance energy transfer experiments, have suggested that rafts in normal unstimulated cells are extremely small and may last for <1 ms (Kenworthy *et al.*, 2004; Kusumi *et al.*, 2004; Sharma *et al.*, 2004). Detergent-resistant membranes have often been regarded as an in vitro correlate of rafts, but detergents themselves have been found to cause domain formation artificially (Heerklotz, 2002). These results have thus posed questions regarding the true existence of rafts in living, nonstimulated cells. In addition, although microscopic identification of rafts has been attempted in a number of studies, putative raft molecules generally show diffuse distribution in the cell membrane without any concentration at the resolution of light microscopy. This result has been interpreted in several different ways, i.e., that rafts do not in fact exist, rafts are too small to be resolved by light microscopy, rafts occupy the majority of the membrane, or rafts do exist but may be disrupted by experimental procedures.

GM1 has been generally regarded as an authentic raft molecule, and cholera toxin B-subunit (CtxB) has been used to probe its distribution in many microscopic studies including FRET (Kenworthy *et al.*, 2000; Nichols, 2003). However, because CtxB is a pentameric molecule that can bind to five GM1 molecules, binding of CtxB itself is likely to change the distribution of GM1 in the membrane as shown for membrane proteins that were cross-linked with antibodies (Mayor *et al.*, 1994; Fujimoto, 1996). Some studies used specimens that were fixed before the CtxB labeling (Parton, 1994), but chemical fixatives are unlikely to preserve the in situ localization of membrane molecules, particularly lipids, and may even cause artifactual results (Jost *et al.*, 1973; Chandler, 1984).

This article was published online ahead of print in *MBC in Press* (http://www.molbiolcell.org/cgi/doi/10.1091/mbc.E07-01-0071) on March 28, 2007.

[D] The online version of this article contains supplemental material at *MBC Online* (http://www.molbiolcell.org).

Address correspondence to: Toyoshi Fujimoto (tfujimot@med.nagoya-u.ac.jp).

Abbreviations used: b-CtxB, biotinylated cholera toxin B; CI, confidence interval; CSR, complete spatial randomness; EM, electron microscopy; GAR-Fab5, colloidal gold (5-nm)-conjugated anti-rabbit IgG F(ab')2 fragment; PAG5, colloidal gold (5-nm)-conjugated protein A; MβCD, methyl-β-cyclodextrin; NND, nearest neighbor distance; PC, phosphatidylcholine; SDS-FRL, SDS-treated freeze-fracture replicas.

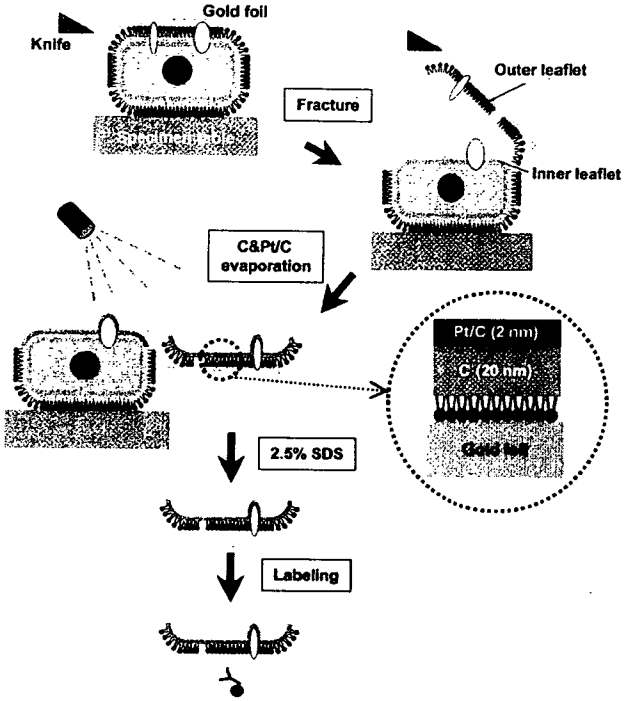

Figure 1. Outline of the SDS-FRL technique used in the present study. Cells cultured on thin gold foils were quick-frozen and freeze-fractured. Replicas were made by evaporation of carbon followed by platinum/carbon in most experiments. The replicas were treated with SDS and labeled with antibodies.

To avoid the possible artifacts caused by probe binding and chemical fixation, and also to take advantage of the high resolving power of electron microscopy (EM), we turned to immuno-EM using SDS-treated freeze-fracture replicas (SDS-FRL) (Figure 1). In combination with rapid freezing, SDS-FRL can immobilize membrane molecules physically and determine their localization in the nanometer range (Fujimoto, 1995). By use of this method, we wanted to examine whether putative raft lipids are distributed in clusters in the living cell membrane as postulated in the raft hypothesis.

In the present study, we labeled gangliosides GM1 and GM3 in the mouse fibroblast membrane, and we analyzed the result by spatial statistical methods in wide membrane areas. As a result, both GM1 and GM3 were found to form clusters in normal mouse fibroblasts, and their clustering became less obvious after cholesterol depletion. Contrary to the simplest raft hypothesis, dissolution of the cluster upon cholesterol depletion was not complete, and it showed regional heterogeneity; and, unexpectedly, a similar result was observed when cells were cooled on ice before rapid freezing. Additionally, clusters of GM1 and GM3 overlapped only partially, suggesting the presence of heterogeneous microdomains. These observations were discussed with reference to the findings obtained using other methodologies.

MATERIALS AND METHODS

Antibodies and Probes

Rabbit anti-GM1 antibodies were raised and affinity-purified as described previously (Kusunoki *et al.*, 1996). Two different batches of antibodies were used in the present study, and they gave equivalent results. Mouse anti-GM3 antibody (clone GMR6; Seikagaku-Kogyo, Tokyo, Japan) and biotin-conjugated cholera toxin B-subunit (b-CtxB; Invitrogen, Carlsbad, CA) were purchased. Mouse anti-phosphatidylcholine (PC) antibody (JE-1) (Nam *et al.*, 1990) was kindly donated by Dr. Masato Umeda (Kyoto University). Secondary antibodies conjugated with fluorochromes (Invitrogen), horseradish peroxidase (Pierce Chemical, Rockford, IL), and colloidal gold (BioCell, Cardiff, United Kingdom), and protein A coupled to colloidal gold (University Medical Center Utrecht, Utrecht, The Netherlands) were obtained from respective suppliers.

Cells

Fibroblasts were explanted from the dermis of wild-type mice and mice lacking the β1,4-*N*-acetylgalactosamine-transferase gene (Takamiya *et al.*, 1996). They were maintained in DMEM supplemented with 10% fetal calf serum, 50 U/ml penicillin, and 0.05 mg/ml streptomycin at 37°C under 5% CO_2, 95% air. The latter cells were referred to as GM1-null fibroblasts. To load GM1-null cells with exogenous GM1 (Sigma-Aldrich, St. Louis, MO), the cells were incubated in serum-free DMEM containing GM1 (0.3, 3, or 30 μM) for 1 h at 37°C in the CO_2 incubator. After incubation, the cells were washed twice with phosphate-buffered saline (PBS) and incubated with PBS containing 0.2% fatty acid-free bovine serum albumin (BSA) (Wako Pure Chemicals, Osaka, Japan) to remove GM1 loosely bound to the cell surface (Schwarzmann *et al.*, 1983). For cholesterol depletion, cells were treated with 5 mM methyl-β-cyclodextrin (MβCD) in DMEM for 60 min.

Thin-Layer Chromatography (TLC) Immunoblotting and Dot Blotting

Total lipids were extracted from cells by using chloroform/methanol, and glycosphingolipids were obtained by reverse phase chromatography with Sep-Pak C18 cartridge (Waters, Milford, MA) (Williams and McCluer, 1980). TLC was performed with high-performance TLC plates (Merck, Darmstadt, Germany) with a solvent system of chloroform/methanol/0.25% $CaCl_2$ (60:35:8). For staining by resorcinol, 0.5 μg of gangliosides was loaded. For TLC immunoblotting, 0.25 μg of gangliosides was developed on TLC plates, transferred to polyvinylidene difluoride membranes, and immunolabeled as described previously (Taki and Ishikawa, 1997). For dot blotting, glycosphingolipids were blotted on the nitrocellulose membrane. The signals of blotting were detected using the SuperSignal West Dura Extended Substrate (Pierce Chemical) according to the manufacturer's instruction.

Immunofluorescence Microscopy

Cells cultured on glass coverslips were fixed with buffered 4% formaldehyde, pretreated with 3% BSA, and incubated with antibodies or b-CtxB, followed by the fluorochrome-conjugated secondary reagents. In some experiments, unfixed cells were incubated with the primary probes on ice, fixed, and then labeled by the secondary reagents. The labeled samples were observed by an Axiophot2 microscope (Carl Zeiss, Jena, Germany) equipped with an AxioCam charge-coupled device camera using an Apochromat oil immersion 63× objective lens with a numerical aperture of 1.4. For quantification of filipin labeling intensity, focus was adjusted by rhodamine-phalloidin in the same specimen, and filipin fluorescence was pictured without observation by an identical microscope setting, and analyzed by ImageJ (National Institute of Health, Bethesda, MD).

Quick-Freezing and Freeze-Fracture

Cells grown on a small gold foil (~4 mm^2 in area; 20 μm in thickness) were inverted upon prewarmed 10% gelatin on a gold-plated copper specimen table with the cell side down according to the metal sandwich method (Fujimoto and Fujimoto, 1997). The cell sandwich was slammed onto the copper block precooled to the liquid helium temperature (−269°C) by using the rapid freezing apparatus HIF-4K (Hitachi High-Technologies, Tokyo, Japan).

For freeze-fracturing, the specimens were transferred to a cold stage of a Balzers BAF400 apparatus, and they were fractured at −95°C and ~2×10^{-6} mbar. Replicas of the fractured membrane were made by electron-beam evaporation of platinum/carbon (Pt/C) and carbon (C), and the replica thickness was controlled by a crystal thickness monitor. Three different evaporation protocols were tested: 1) Pt/C (2 nm) followed by C (20 nm), 2) C (20 nm) followed by Pt/C (2 nm), 3) C (2 nm) followed by Pt/C (2 nm), and then by C (20 nm). After thawing, the replicas were immediately treated for 5 min in 2.5% SDS in PBS at 70°C. They were adjusted to 50% glycerol and kept at −20°C until labeling. Immunogold labeling was done as described previously (Fujimoto *et al.*, 1996), and the specimens were observed with a JEOL 1200EX electron microscope operated at 100 kV.

Statistical Analysis of Immunogold Labeling

Electron micrographs were digitized with an image scanner. The *x-y* coordinates of gold particles were obtained by Image Processing Tool Kit version 5 plug-in (Reindeer Graphics, Asheville, NC) for Adobe Photoshop version 6 (Adobe system, Mountain View, CA), and areas of 1 μm × 1 μm chosen randomly were analyzed by Ripley's K-function (Ripley, 1979) by using a program provided by John Hancock (Prior *et al.*, 2003). For significance tests,

99% confidence envelopes for complete spatial randomness (CSR) were generated from 100 Monte Carlo simulations. The frequency distribution of the nearest neighbor distance distribution was obtained by using the Image Processing Tool Kit.

Measurement of Phospholipids Bound to Replicas

The amount of phospholipids retained in SDS-treated C-Pt/C replicas was measured as described previously. Briefly, a suspension of small unilamellar PC liposomes was sandwiched between two thin copper foils, quickly frozen, freeze-fractured, and shadowed. One of the complementary replicas was washed in distilled water, and the other replica was treated with 2.5% SDS and washed with distilled water. The replicas were treated with 70% perchloric acid at 200°C for 2 h, and the released phosphorus was measured (Zhou and Arthur, 1992).

Biochemical Assay of Cholesterol

The total lipids were extracted from cells by a mixture of hexane and isopropanol (3:2), and the amount of free cholesterol was measured by enzymatic fluorometric method as described previously (Heider and Boyett, 1978).

On-Grid Model Experiment

Colloidal gold (2 nm; BioCell) conjugated with recombinant glutathione S-transferase (GST) was applied to Formvar-coated EM grids, blocked, and labeled with rabbit anti-GST followed by GAR-Fab5 or by PAG5. In other experiments, a dilute solution of recombinant GST was put on Formvar-coated grids and labeled by the same protocol.

RESULTS

Antibody Specificity

In enzyme-linked immunosorbent assay analysis with purified gangliosides, one of the two rabbit anti-GM1 antibodies used in our present study reacted with GM1 alone, whereas the other one also bound to GD1b and GA1. However, neither of these GM1 antibodies recognized GM2, GM3, GD1a, GD3, or GT1b (data not shown). In addition, by TLC blotting of gangliosides extracted from mouse fibroblasts, both of these antibodies showed positive reactivity only at the GM1 position and not GD1b or GA1 (Supplemental Figure 1). b-CtxB also reacted at the same position as the anti-GM1 antibodies. The monoclonal anti-GM3 antibody produced a band in cell extracts at the correct GM3 position and not GM1 (Supplemental Figure 1). The bands recognized by anti-GM1 and anti-GM3 antibodies were broader in the cell samples than that were for purified GM1 and GM3 molecules, but this is probably due to the presence of heterogeneous fatty acids, and/or the presence of glycolyl and acetylated forms of sialic acids in fibroblasts.

Immunogold Labeling of Freeze-Fracture Replicas

We previously showed that phospholipids are retained on SDS-treated freeze-fracture replicas and that they can be labeled by antibodies, but the labeling density was relatively low (Fujimoto *et al.*, 1996). To explore different conditions that may facilitate the efficient labeling of GM1, we compared replicas prepared in three different ways. In replicas produced by the conventional evaporation method, e.g., Pt/C (2 nm) followed by C (20 nm), labeling was found to be extremely low either by anti-GM1 antibody or by b-CtxB. The labeling intensity was improved, however, when the replicas were prepared by evaporating C before Pt/C. C (20 nm)-Pt/C (2 nm) replicas and C (2 nm)-Pt/C (2 nm)-C (20 nm) replicas gave equivalent results (Supplemental Figure 2). The retention of phospholipids in the SDS-treated replicas was not compromised by the change of the evaporation method: 82.6 ± 13.0% (n = 3) phosphatidylcholine was retained in the C (20 nm)-Pt/C (2 nm) replicas, which was even better than the retention ratio obtained for the conventional Pt/C (2 nm)-C (20 nm) replicas (Fujimoto *et al.*, 1996). Although the structural details became somewhat less defined in the C (20 nm)-Pt/C (2 nm) replica, we adopted this method in the present study due to its simplicity. Regardless of the procedure that was used for replica preparation, the labeling of GM1 was observed only in the E face, which represents the outer leaflet, and not in the P face, which represents the inner leaflet, or in the cytoplasm (Figure 3A, inset). Because the rabbit anti-GM1 antibodies gave significantly better labeling than b-CtxB, we used these antibodies in all of the subsequent EM experiments. The labeling efficiency of GM1 by the current method was calculated as described in Supplemental Table 1, and it was estimated that no less than 19.4% of GM1 in the original membrane was captured by immunogold labeling on the replicas.

The specificity of labeling in the replicas was confirmed using GM1-null cells (Takamiya *et al.*, 1996). Replicas of those cells were devoid of labeling either by the anti-GM1 antibodies or by b-CtxB (Figure 2C). Significantly, however, positive labeling by both probes was observed when exogenous GM1 was added to the culture medium before freezing. The quantitative loading of GM1 was confirmed by dot blotting and immunofluorescence microscopy (Figure 2, A and B), and the density of replica labeling increased as the GM1 concentration in the medium was raised from 0.3 to 30 μM (Figure 2C). The distribution of the labeling in the GM1-loaded cells was indistinguishable from that in normal mouse fibroblasts. Detailed analysis of the labeling is described below. Because the current methodology precludes the observation of molecules outside the lipid bilayer, the aforementioned results also demonstrate that exogenous GM1 molecules are incorporated into the cell membrane and that they adopt a similar disposition to endogenous GM1.

Distribution of GM1 in the Cell Membrane

By use of the aforementioned technique, GM1 distribution in normal mouse fibroblasts was examined. Immunogold labeling gave apparently clustered distribution (Figure 3A). To obtain objective data, 50 areas of 1 × 1 μm were randomly chosen from samples obtained in more than three independent experiments, and the distribution patterns were assessed by point pattern analysis using Ripley's K-function (Ripley, 1977, 1979; Prior *et al.*, 2003). When all the samples were compiled, the $L(r) - r$ curve was found to deviate most from the 99% confidence interval (CI) at a radius of 47.0 nm (Figure 3B). When individual samples were analyzed, the $L(r) - r$ curve showed a prominent peak except in a few cases (Supplemental Figure 3), and the peak size ranged from 32 to 68 nm (Figure 3C). We assumed that the basic cluster is in this size range (the size includes the arm length of the antibodies, which will be discussed later), and in subsequent experiments we classified the GM1 distribution patterns as "clustered" when the K-function was above the 99% CI at more than one point below a 100-nm radius. By this criterion, the GM1 labeling was clustered in all of the randomly chosen areas (50/50). The density of immunogold particles per unit area was found to be quite variable (Figure 4F), but GM1 clustering was observed irrespective of the labeling density.

The aforementioned result was obtained using rabbit anti-GM1 as the primary antibody, and colloidal gold (5 nm)-conjugated anti-rabbit IgG F(ab')2 fragment (GAR-Fab5) as the secondary probe. Because of the small size of the GM1 head group and the highly selective binding characteristics of the anti-GM1 antibody, it is unlikely that more than two primary antibodies bound to a GM1 molecule. In contrast, more than two GAR-Fab5 particles could bind to a primary antibody. However, we concluded that the clustering of GM1 labeling was not due to multivalency based on the

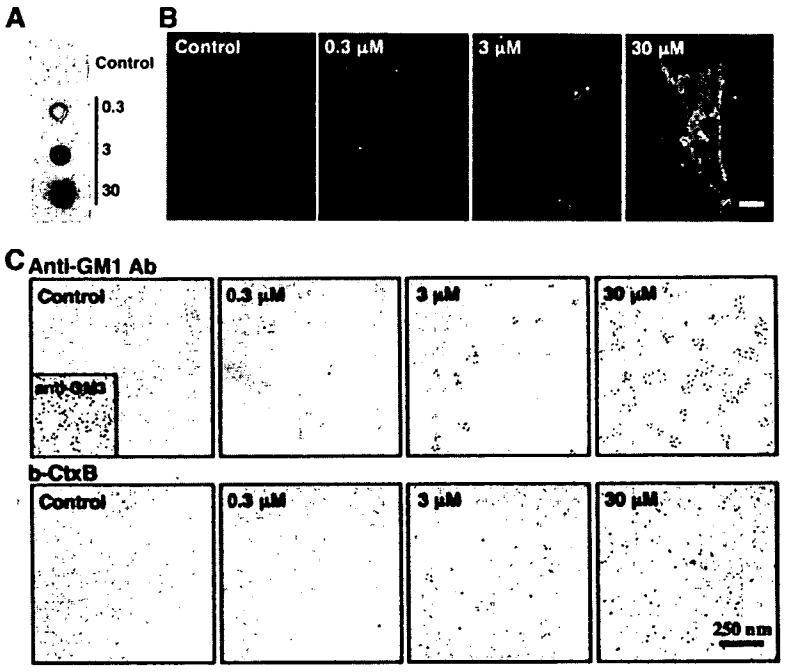

Figure 2. Fibroblasts obtained from GM1-null mice were cultured with or without 0.3, 3, or 30 μM GM1 for 60 min. (A) Dot blot labeling by b-CtxB. (B) Fluorescence microscopy using b-CtxB, followed by fluorescein isothiocyanate-avidin. The addition of GM1 to the culture medium increases the GM1 content in GM1-null mouse fibroblasts. Scale bar, 10 μm. (C) Freeze-fracture replicas were labeled by anti-GM1 antibody (top row), or by b-CtxB (bottom row). With either probe, labeling was not observed without GM1 loading, and labeling increased according to the amount of loading. Labeling of GM3 was observed without GM1 loading (inset). Ten-nanometer colloidal gold was used for labeling.

following results. First, a model experiment showed that two or three GAR-Fab5 particles could bind to an IgG molecule in 15.7 and 3.6% of the cases, respectively. When random point patterns were generated and the above-mentioned proportions of points were duplicated or triplicated, however, the resultant patterns did not show clustering as analyzed by Ripley's K-function (Supplemental Figure 4). Second, a very similar clustering was obtained when using colloidal gold (5 nm)-conjugated protein A (PAG5) as the secondary probe (Supplemental Figure 5, A and B). Only one PAG5 particle should bind to an IgG molecule, and the result of the model experiment was consistent with this principle (Supplemental Figure 4).

We next analyzed the entire area of randomly chosen cells to examine possible local heterogeneity within a single cell. Replicas were often disrupted within the cellular boundary, but areas of 145 μm^2 (ranging from 55 to 327 μm^2) could be observed on average for each cell. From this analysis, 70% of the cells showed only a clustered distribution throughout their surface, but the remainder showed small areas of random distribution (Figure 4D). An example of a whole cell profile and local $L(r) - r$ curves is shown in Supplemental Figure 6.

Effects of Cholesterol Depletion and Low Temperatures on GM1 Clustering

We next examined distribution of GM1 in mouse fibroblasts after depleting cholesterol to disrupt rafts. In cells treated with 5 mM MβCD for 60 min, the free cholesterol content was reduced considerably (Supplemental Figure 7). In these cells, 28% (14/50) of the areas showed random GM1 distribution, but 72% (36/50) still showed clustering (Figure 4C). Essentially, the same result was obtained when PAG5 was used for labeling (Supplemental Figure 5, B and C). Analysis of the compiled data also showed clustering (Figure 4A), but when individual samples were assessed, the peak of the $L(r) - r$ curves was clearly lower, broader, and less distinct compared with the control sample (Supplemental Figure 3).

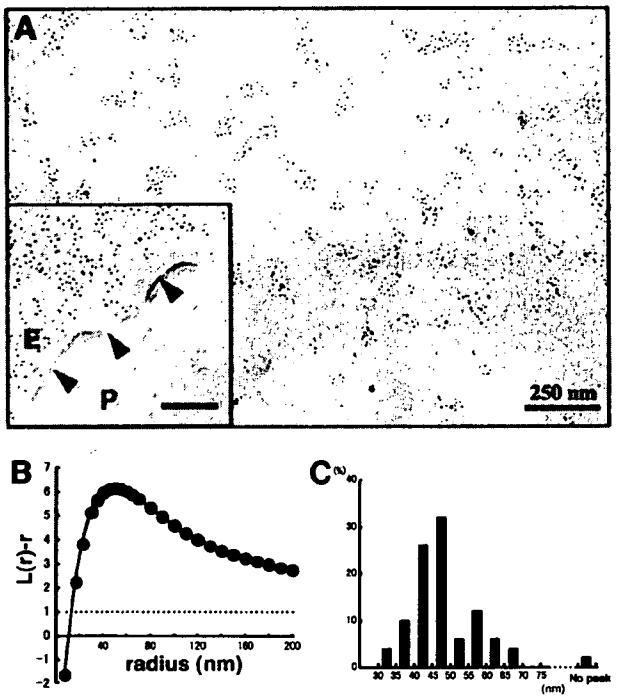

Figure 3. Labeling of freeze-fracture replicas of normal mouse fibroblasts by rabbit anti-GM1 antibody and colloidal gold (5-nm)-conjugated anti-rabbit IgG F(ab')2 fragment (GAR-Fab5). (A) GM1 labeling by 5-nm colloidal gold particles was detectable as clusters in the E face of the freeze-fractured plasma membrane. Inset, the P face was unlabeled. The cell boundary is marked by arrowheads. Ten-nanometer colloidal gold was used for labeling in this sample. (B) Fifty areas (1 × 1 μm) were randomly photographed, and the gold point patterns were analyzed by Ripley's K-function. The mean $L(r) - r$ curve showed maximal deflection from CSR (99% CI is shown by a dotted line) at a 47.0-nm radius. (C) Radii of maximal deflection for 50 sample areas ranging from 32 to 68 nm, with only one area showing no apparent peak.

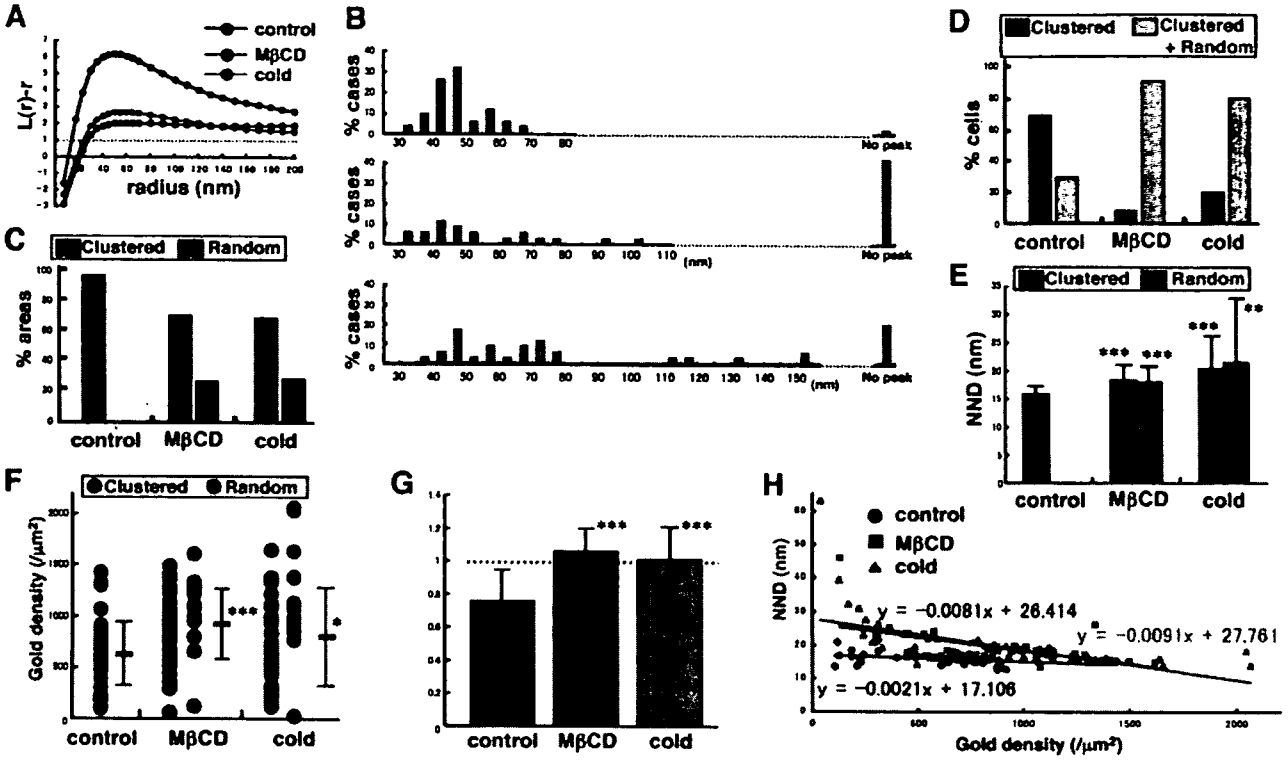

Figure 4. Analysis of GM1 distribution in normal mouse fibroblasts under three different conditions: control, cholesterol depletion, and incubation on ice for 30 min. (A) Mean $L(r) - r$ curves. The pooled data show clustering even after cholesterol depletion or chilling, but deviation from CSR was considerably smaller than the control. (B) Radii of maximal deflection in 50 areas. $L(r) - r$ curves without any peak below $r = 200$ nm increased after either treatment. (C) Classification based on K-function analysis. Areas showing more than one point above the 99% CI below $r = 100$ nm were regarded as clustered. (D) Classification of 10 randomly chosen cells. The entire area in each cell was analyzed. Cells were classified by whether they showed clustered areas only or both clustered and random areas. (E) NND analysis. NND values increased significantly after cholesterol depletion or chilling, compared with control cells (Student's t test; $^{**}p < 0.005$, $^{***}p < 0.001$). (F) The average labeling density showed a wide range for each sample and increased significantly after cholesterol depletion or chilling (Student's t test; $^{*}p < 0.05$, $^{***}p < 0.001$). (G) NND normalized to the value expected for random distribution. Only the control sample showed a value significantly <1 ($^{***}p < 0.001$). (H) Correlation of NND and the average labeling density. The dependence of NND upon the labeling density was far less in the control than in the treated samples.

In cholesterol-depleted wild-type mouse fibroblasts, the clustered and random distribution patterns of GM1 coexisted in >90% of the cells (Figure 4D). As shown in representative cases (Figure 5 and Supplemental Figure 6), the two different patterns were often observed side by side in narrow areas of the membrane. The result confirmed that the clustering of GM1 was not caused artifactually by the experimental procedures after freezing.

With the assumption that a low temperature would increase the raft area, and thus induce a further GM1 clustering, we kept mouse fibroblasts on ice for 30 min before rapid freezing. In contrast to the assumption, however, the distribution of the GM1 labeling in those cells showed changes that were very similar to those observed in cholesterol-depleted cells. The areas showing both clustered and random GM1 patterns were 70% (35/50) and 30% (15/50), respectively (Figure 4C). Individual samples also revealed a similar tendency, and the $L(r) - r$ curves generally became less distinct and broader than the control (Supplemental Figure 3). The coexistence of both clustered and random distribution patterns of GM1 in these cells was also observed in 80% of cases (Figure 4D). The changes caused by the cold were not likely to be caused by energy depletion because treatment with 10 mM sodium azide and 10 mM 2-deoxyglucose for 30 min, which inhibited endocytosis of CtxB completely, did not affect the GM1 distribution (data not shown).

Cholesterol depletion and low temperatures caused similar changes in two other indices: both the nearest neighbor distance (NND) and the average labeling density values increased significantly (Figure 4, E and F). The average NND, normalized to the value expected for random distribution, was significantly <1 in the control cells, but it became close to 1 after either cholesterol depletion or chilling (Figure 4G). Most significantly, the NND was virtually independent of the labeling density in control cells, whereas the NND decreased as the labeling density increased in cells after cholesterol depletion or chilling (Figure 4H). These data strongly indicate that GM1 in control mouse fibroblasts is clustered and that it becomes less so after cholesterol depletion or chilling.

The changes caused by cholesterol depletion and the cold were observed similarly in GM1-null cells preloaded with 10–15 μM GM1. The peak of the $L(r) - r$ curves became lower (Figure 6A), the frequency of random areas increased (Figure 6B), and the average labeling density increased (Figure 6C). Cholesterol depletion caused a more drastic change in the GM1-loaded cells than in the normal mouse fibroblasts. The reason is not clear, but some difference in the fatty acid composition between exogenous GM1 derived

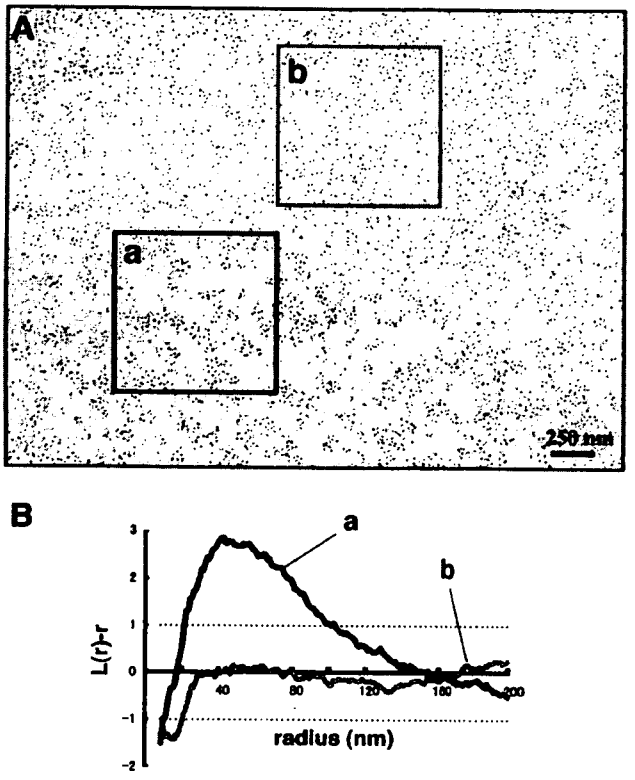

Figure 5. GM1 labeling in mouse fibroblasts treated with 5 mM MβCD for 60 min. (A) The labeling shows a marked regional heterogeneity in most cells. (B) The gold point patterns of adjacent areas in A show clustered (a) and random (b) distributions, respectively.

from bovine brain and GM1 expressed endogenously in mouse fibroblasts may be involved.

As a control, PC was labeled by SDS-FRL. Probably because the epitope of the anti-PC antibody includes a hydrophobic portion of PC that is located deeper in the lipid bilayer (Nam *et al.*, 1990), the antibody can only bind to a certain population of PC molecules, and the labeling does not occur homogenously even on liposome replicas (see figure 2A of Fujimoto *et al.*, 1996). A similar patchy labeling pattern was observed in the mouse fibroblast (Figure 7A). In contrast to GM1 (Figure 3) and GM3 (see below), the distribution of the PC labeling was not affected by cholesterol depletion, whereas chilling caused reduction of clustering (Figure 7B). Because of the unidentified binding characteristics of the anti-PC antibody, definite interpretation of the result is not possible, but the result showed that the distributional changes do not occur in the same manner in membrane lipids.

Distribution of GM3 in Relation to GM1

We next examined distribution of another ganglioside, GM3, by the same technique. GM3 also showed a clustered pattern in normal mouse fibroblasts (Figure 8). In comparison with GM1, the $L(r) - r$ curve of the GM3 labeling did not show an evident peak (Figure 8A), indicating that the size of the GM3 cluster was highly variable and generally larger than that of the GM1 cluster. We confirmed that the indirect immunolabeling protocol, i.e., mouse immunoglobulin M (IgM) followed by colloidal gold-conjugated anti-mouse Ig antibody, did not cause prominent clustering by a model experiment similar to Supplemental Figure 4 (data not shown). In cells depleted of cholesterol by MβCD, the clustering of GM3 decreased significantly (Figure 8B). According to the criterion used for GM1, 26.7% (8/30) of the area showed random distribution, and in the rest of the cases, the $L(r) - r$ curve was out of the CI range (Figure 8C). But as in the case of GM1, analysis of the individual areas showed that the $L(r) - r$ curves became generally lower in cholesterol-depleted cells even when they were classified as "clustered" by the criterion used for GM1 (Supplemental Figure 8). These results indicated that the clustering of GM3 is also related to the cholesterol content of the plasma membrane.

The relationship between the GM1 and GM3 clusters in normal mouse fibroblasts was examined by double labeling by using colloidal gold particles of two different diameters. By use of the bivariate K-function, two different patterns were observed. In a relatively limited number of areas (13.3%), GM1 and GM3 were observed to make coclusters,

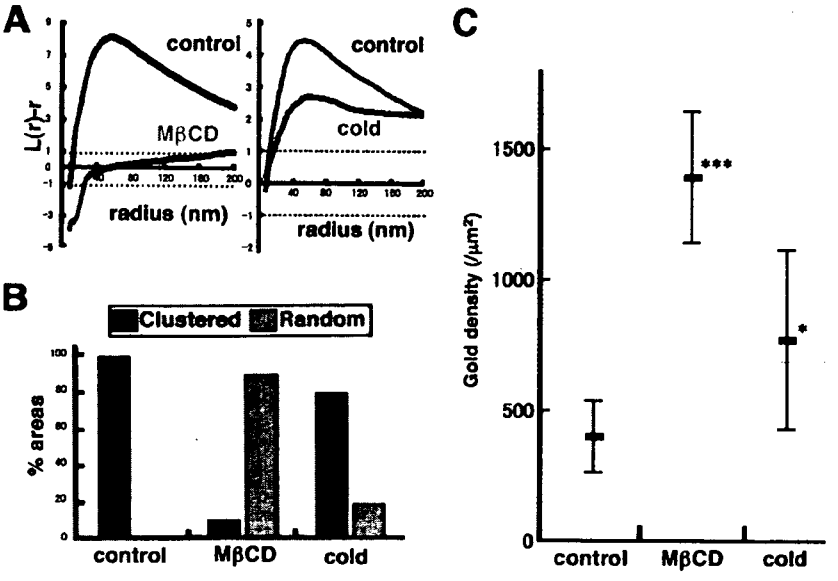

Figure 6. Changes observed after cholesterol depletion and chilling in normal mouse fibroblasts were also observed in GM1-null fibroblasts loaded with exogenous GM1. (A) The mean $L(r) - r$ curve shows a decrease of clustering after cholesterol depletion by MβCD or after chilling. The change was more drastic by cholesterol depletion than by chilling. (B and C) The proportion of areas showing random distribution as well as the average labeling density also increased significantly by cholesterol depletion or chilling.

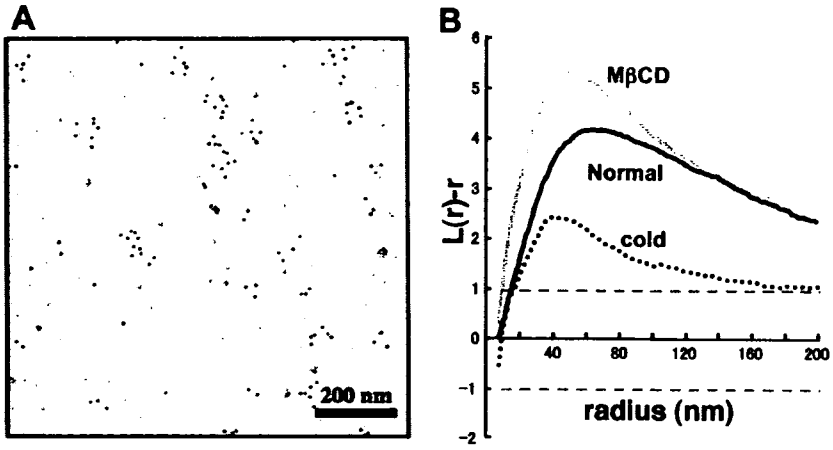

Figure 7. Distribution of PC labeled by mouse anti-PC antibody (IgM) and colloidal gold (5-nm)-conjugated goat anti-mouse Ig antibody. (A) The labeling of PC in the normal mouse fibroblast was observed as clusters in the E face, which was similar to that seen in liposomes and in other cell types (Fujimoto *et al.*, 1996). (B) The K-function analysis of 10 areas (1 × 1 μm) showed that the labeling was clustered in the normal mouse fibroblast. The clustering was observed similarly in cells depleted of cholesterol, but it decreased in chilled cells.

whereas in most areas (86.7%), the GM1 and GM3 clusters were segregated and formed independently (Figure 9, A and B). When coclustering was observed, GM1 clustering was less discrete than that observed by single labeling, which was evident in the $L(r) - r$ curve of the univariate K-function analysis (data not shown). This difference was likely caused by steric hindrance between the anti-GM1 and anti-GM3 antibodies binding to overlapping areas.

DISCUSSION

Methodological Considerations

SDS-FRL has several advantages for analyzing the distribution of membrane molecules in the submicrometer range. By freezing live cells quickly to the liquid helium temperature, the molecular motion in the cell should stop immediately. Phase separation may occur in membranes that were cooled slowly, but it was prevented by this quick-freeze method (Thompson *et al.*, 1985). In their pioneering article, Heuser and his colleagues showed that the surface of a muscle piece became frozen within 1 ms after the impact with the liquid helium-cooled copper block (Heuser *et al.*, 1979). They later found that the freezing rate is at least 10 times faster than that (Heuser, personal communication). Although details in the present experiment were different from their experiment, the cell membrane of thin culture cells should be frozen at a better cooling rate than the muscle piece. Further sophistication in the measurement of the freezing rate is required to assess the time and spatial resolution of this method precisely.

During the freeze-fracture procedure, the specimens were kept frozen below −100°C, and the fractured membrane half was coated by evaporation of C and Pt/C to immobilize membrane molecules in situ. The physical fixation provided by the combination of quick-freezing and freeze-fracturing contrasts with chemical fixation by aldehydes in many respects. Aldehydes have only limited reactivity with membrane lipids and could even cause redistribution of membrane proteins by a cross-linking effect (Kusumi and Suzuki, 2005). More than several seconds are required for the aldehyde fixation to complete, and even after fixation, membrane molecules retain their two-dimensional mobility (Jost *et al.*, 1973; Chandler, 1984). Thus, in specimens fixed by formaldehydes, binding of probes, especially multivalent probes, could cause redistribution of membrane molecules (Mayor *et al.*, 1994). Although glutaraldehyde was shown to prevent gross redistribution of membrane proteins (Mayor *et al.*, 1994), it is unlikely to stabilize membrane lipids in the nanometer range. The membranes stabilized in replicas preclude the possibility of such artifacts caused by probes.

Compared with the conventional method that evaporates Pt/C before C, the labeling of gangliosides was improved drastically by evaporating C before Pt/C. A similar effect has been reported for some membrane proteins (Hagiwara *et*

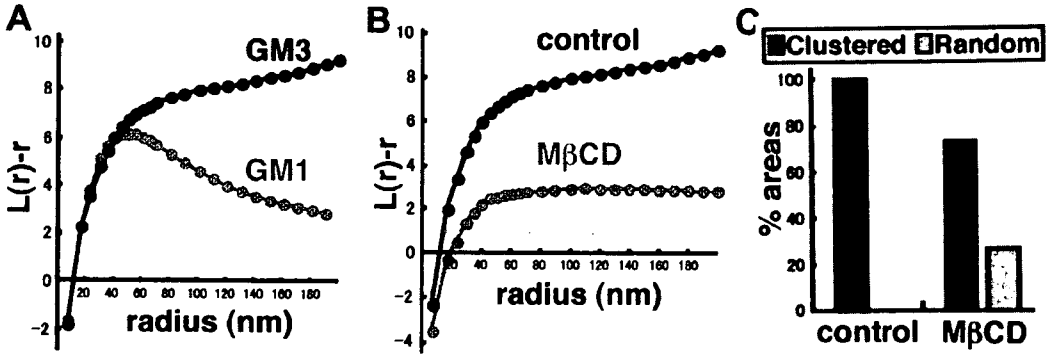

Figure 8. GM3 labeling in normal mouse fibroblasts. (A) Thirty randomly chosen areas (1 × 1 μm) were analyzed by Ripley's K-function. In contrast to GM1, the mean $L(r) - r$ curve of GM3 did not show any apparent deflection below r = 200 nm. (B) The mean $L(r) - r$ curve became lower after cholesterol depletion. (C) Classification of the 30 areas according to K-function analysis. Cholesterol depletion caused an increase in the number of areas with random distribution.

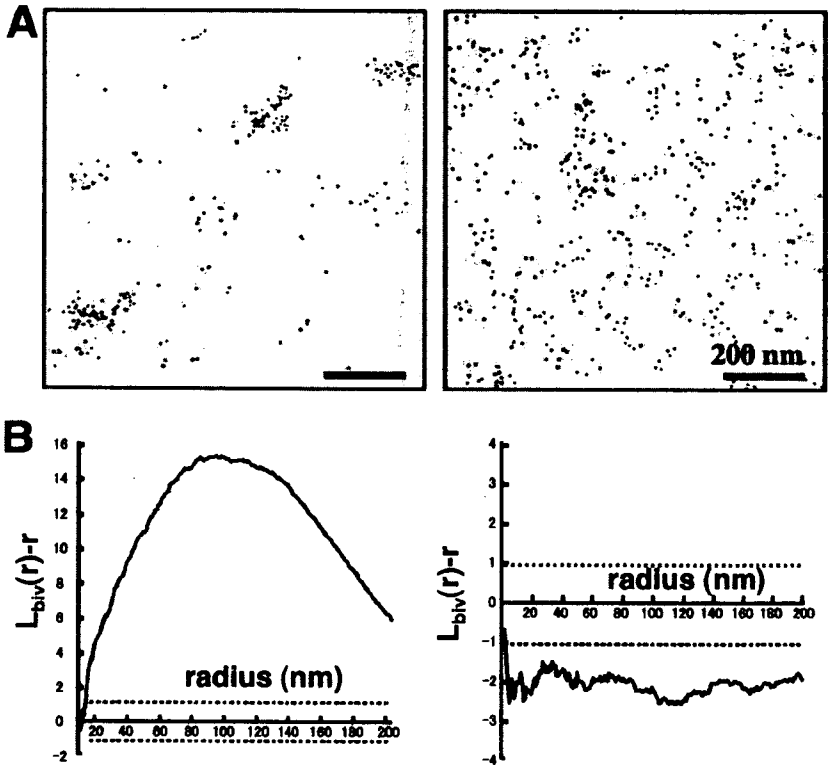

Figure 9. Double labeling of GM1 and GM3 in normal mouse fibroblasts. (A) GM1 and GM3 were marked with colloidal gold particles of different sizes, which were colored artificially: GM1, black; GM3, orange. (B) Analysis of the two areas shown in A by using a bivariate K-function. GM1 and GM3 were found to be coclustered in the left sample, but they segregated from each other in the right sample. Coclustering as shown in the left graph was seen only in 13.3% of the cases.

al., 2005). The reason for this improvement is not fully clear, but compared with Pt/C, pure C casting may allow the molecules to retain some flexibility, which may facilitate their interaction with probes. Additionally, the use of antibodies improved the GM1 labeling in SDS-FRL. CtxB worked well for immunofluorescence microscopy, but it labeled the replica to a much lesser extent than the anti-GM1 antibodies. For high-affinity binding of pentameric CtxB molecules, GM1 molecules and surrounding lipids may need to be rearranged properly, and this probably occurs frequently in the fluid membrane. The relatively low labeling by SDS-FRL may have resulted because molecules in the replica are immobilized, and they do not take an appropriate arrangement very often.

GM1 Clustering in the Cell Membrane

The GM1 labeling formed clusters with an average radius of 47.0 nm in control mouse fibroblasts. The average labeling density ranged from <100 to >1400 particles/μm^2, but clusters of similar sizes were observed irrespective of the GM1 density. In our present method, two layers of probes, either a whole IgG molecule and a F(ab')2 portion (GAR-Fab5) or a whole IgG and protein A (PAG5), were intercalated between colloidal gold (5 nm) and the antigen. Using a model experiment, the spacer distances were estimated as 16.3 ± 4.1 nm (GAR-Fab5) and 16.1 ± 5.3 nm (PAG5) (Supplemental Figure 10). This lead to a calculated size of the GM1 cluster of ~61 nm in diameter, which roughly corresponds to that which was estimated by several studies for glycosylphosphatidylinositol (GPI)-anchored protein clusters (Friedrichson and Kurzchalia, 1998; Varma and Mayor, 1998; Pralle *et al.*, 2000), but it is larger than the estimate obtained in more recent studies by using sophisticated biophysical techniques (Kusumi *et al.*, 2004; Sharma *et al.*, 2004). Ras proteins were also shown to make smaller clusters by immuno-EM of mechanically detached membranes (Plowman *et al.*, 2005). The size difference of the clusters is not surprising, however, because GPI-anchored proteins were shown to behave differently from GM1 in several instances (Schnitzer *et al.*, 1995; Simons *et al.*, 1999; Dietrich *et al.*, 2001b). It is also likely that the Ras cluster in the inner leaflet does not coincide with that of GM1 in the outer leaflet. SDS-FRL should be able to study the distribution of those proteins and to compare the cluster sizes directly.

After cholesterol depletion or incubation of cells on ice, GM1 labeling became less clustered, and areas showing random distribution increased significantly. In addition, cholesterol depletion and chilling increased the average labeling density as well as the NND. The increase of the labeling density could reflect a real increase of GM1 molecules in the plasma membrane, but the change of the aforementioned three parameters together, and above all, the virtual independence of NND values from the labeling density in control cells (Figure 4H), is more likely to suggest a dispersion of GM1 clusters by cholesterol depletion or by chilling. That is, GM1 molecules densely packed in control cells are probably not labeled efficiently due to steric hindrance, but after cholesterol depletion or chilling, they may be dispersed and more GM1 molecules may become accessible to antibodies. This possibility also suggests that the density of GM1 molecules in the cluster is underestimated in immunogold labeling.

An important question that arises from our current data is the very nature of these GM1 clusters. The clusters may be explained by the presence of rafts, or liquid-ordered (*lo*) domains, and by preferential partitioning of GM1 in the domains. The results of our chilling experiments would not seem consistent with this supposition, because low temperatures are expected to increase more ordered domains,

whereas cholesterol depletion should disrupt *lo* domains (Simons and Ikonen, 1997; Gaus *et al.*, 2003). However, as the temperature is decreased, the *lo* domain should become the dominant or percolating phase, and GM1 and other raft-philic molecules that are confined to small nonpercolating *lo* domains at the ambient temperature may adopt a dispersed distribution in the expanded *lo* domains (Meder *et al.*, 2006). Hence, the dispersed GM1 distribution after chilling can be interpreted to reflect the larger *lo* domain, or an increase of raft areas. This contrasts with the similarly dispersed GM1 distribution after cholesterol depletion, which may be caused by an increase of the liquid-disordered domains, or disruption of rafts.

However, the incomplete dissolution of the GM1 cluster and the marked regional heterogeneity upon cholesterol depletion suggest that preferential partitioning in the ordered membrane may not explain the whole phenomenon. In this context, it is notable that several studies showed formation of GM1-rich microdomains within the ordered phase of model membranes (Vie *et al.*, 1998; Yuan and Johnston, 2000; Yuan *et al.*, 2002), suggesting that glycolipids are capable of self-organization (but please note that other studies failed to observe the clustering of charged gangliosides; Thompson *et al.*, 1985; Wang and Silvius, 2003). Furthermore, the extracellular matrix, the cytoskeleton, and membrane proteins may influence distribution of membrane molecules in various ways (Edidin, 2003; Ritchie *et al.*, 2003; Mukherjee and Maxfield, 2004). These results raised a possibility that those nonraft factors are sufficient to generate the GM1 cluster in mouse fibroblasts and that rafts are not involved. Under this conjecture, the result of cholesterol depletion might be attributed to its effect on the actin cytoskeleton (Kwik *et al.*, 2003). However, we observed that manipulation of actin filaments did not affect the GM1 distribution to the extent that can explain the result of cholesterol depletion (Fujita, Cheng, and Fujimoto, unpublished observation). Moreover, chilling is not likely to affect the actin cytoskeleton in the same manner. We thus inferred that preferential partitioning in the ordered membrane is involved at least partially for the generation of GM1 clusters.

Irrespective of the mechanism that facilitates GM1 clustering in living cells, the present result has several implications. First, it has not been easy to understand why cholesterol depletion and chilling could both activate mitogen-activated protein kinase signaling (Furuchi and Anderson, 1998; Kabouridis *et al.*, 2000; Chen and Resh, 2002; Gousset *et al.*, 2002; Magee *et al.*, 2005), because the two manipulations are thought to exert opposite effects on rafts, but the present result on GM1 suggests that the two manipulations may affect the distribution of individual raft-philic molecules in the same manner and could cause a similar outcome. This tenet may be tested directly by probing fine distribution of signaling proteins that reside in the inner leaflet of the cell membrane. Second, cooling on ice has been often used to label cells for microscopy with the tacit supposition that the molecular distribution at an ambient temperature is retained. However, the present results indicated that cooling could change the distribution of some membrane molecules, so data that have been obtained from chilled cells need to be interpreted with caution.

Heterogeneous Clusters of GM1 and GM3

We observed that both GM1 and GM3 formed clusters susceptible to cholesterol depletion in normal mouse fibroblasts but that the respective clusters were segregated from each other in most cases. In migrating T cells, a distinct segregation of GM1 and GM3, i.e., GM1 in the uropod and GM3 in the leading edge, was observed (Gomez-Mouton *et al.*, 2001). Our result suggests that GM1 and GM3 also distribute differentially in other cell types, although on a much more minuscule scale. The result also implies that the high distribution density of the two gangliosides has precluded the observation of their segregation by light microscopy in the past.

Biochemical fractions enriched with GM1 and GM3 have been shown to contain different sets of signaling molecules (Iwabuchi *et al.*, 1998; Chigorno *et al.*, 2000). Those fractions are likely to correspond to the GM1 and GM3 domains that we observed, and this would raise two immediate questions. One question is whether the spatial relationship of the two domains would modulate signaling by altering molecular interactions among the signaling proteins. We observed occasional coclustering of GM1 and GM3, which suggests that the two domains could coalesce under certain conditions. It would be interesting to study how coalescence and segregation of those domains are regulated and what is brought about as a result of the domain interactions. The second question is how signaling proteins in the inner leaflet partition to one of the ganglioside domains preferentially. This may be related to the mechanism that generates separate clusters of GM1 and GM3. An intriguing possibility is that GM1 and GM3 are diversified in the ceramide portion and thus favor homologous interactions (Sonnino and Chigorno, 2000; Hakomori Si, 2002). This is not an unrealistic speculation, because glycosyltransferases for the late ganglioside biosynthetic pathways are in the distal Golgi membranes (Lannert *et al.*, 1998), which harbor cholesterol-dependent microdomains, and the probability that a GM3 molecule is processed to become GM1 may depend on the affinity of its ceramide portion to the microdomain where the enzymes exist. As a result, gangliosides remaining as GM3, and those that became GM1, are likely to make homologous clusters more often than heterogeneous gangliosides. Analysis of the ceramide composition of gangliosides is awaited to test the possibility.

Although the underlying mechanism needs to be explored further, our result showed that GM1 and GM3 exist as distinct clusters in the native cell membrane. But the GM1 and GM3 clusters may not be the only microdomains that are affected by cholesterol depletion, and additional microdomains with variable contents are likely to coexist (Marwali *et al.*, 2003; Nagatsuka *et al.*, 2003; Brugger *et al.*, 2004; Kiyokawa *et al.*, 2005). How all those heterogeneous microdomains are formed and how their mutual relationship is controlled warrant further investigation. Hopefully, the present method would help to address these unsolved questions in the near future.

ACKNOWLEDGMENTS

We thank Drs. Atsuyuki Okabe and Ken-ichiro Shimatani for advice on point pattern analysis, Dr. John Hancock for providing the K-function program, Dr. Masato Umeda for anti-PC antibody, Drs. Akihiro Kusumi and John E. Heuser for helpful discussions, and Kumi Tauchi-Sato and Tetsuo Okumura for assistance. This work was supported by grants-in-aid for scientific research and the 21st Century Center of Excellence Program "Integrated Molecular Medicine for Neuronal and Neoplastic Disorders" of the Ministry of Education, Culture, Sports, Science and Technology of the Japanese Government.

REFERENCES

Brugger, B., Graham, C., Leibrecht, I., Mombelli, E., Jen, A., Wieland, F., and Morris, R. (2004). The membrane domains occupied by glycosylphosphatidylinositol-anchored prion protein and Thy-1 differ in lipid composition. J. Biol. Chem. *279*, 7530–7536.

Chandler, D. E. (1984). Comparison of quick-frozen and chemically fixed sea-urchin eggs: structural evidence that cortical granule exocytosis is preceded by a local increase in membrane mobility. J. Cell Sci. *72*, 23–36.

Chen, X., and Resh, M. D. (2002). Cholesterol depletion from the plasma membrane triggers ligand-independent activation of the epidermal growth factor receptor. J. Biol. Chem. *277*, 49631–49637.

Chigorno, V., Palestini, P., Sciannamblo, M., Dolo, V., Pavan, A., Tettamanti, G., and Sonnino, S. (2000). Evidence that ganglioside enriched domains are distinct from caveolae in MDCK II and human fibroblast cells in culture. Eur. J. Biochem. *267*, 4187–4197.

Dietrich, C., Bagatolli, L. A., Volovyk, Z. N., Thompson, N. L., Levi, M., Jacobson, K., and Gratton, E. (2001a). Lipid rafts reconstituted in model membranes. Biophys. J. *80*, 1417–1428.

Dietrich, C., Volovyk, Z. N., Levi, M., Thompson, N. L., and Jacobson, K. (2001b). Partitioning of Thy-1, GM1, and cross-linked phospholipid analogs into lipid rafts reconstituted in supported model membrane monolayers. Proc. Natl. Acad. Sci. USA *98*, 10642–10647.

Edidin, M. (2003). The state of lipid rafts: from model membranes to cells. Annu. Rev. Biophys. Biomol. Struct. *32*, 257–283.

Friedrichson, T., and Kurzchalia, T. V. (1998). Microdomains of GPI-anchored proteins in living cells revealed by crosslinking. Nature *394*, 802–805.

Fujimoto, K. (1995). Freeze-fracture replica electron microscopy combined with SDS digestion for cytochemical labeling of integral membrane proteins. Application to the immunogold labeling of intercellular junctional complexes. J. Cell Sci. *108*, 3443–3449.

Fujimoto, K., Umeda, M., and Fujimoto, T. (1996). Transmembrane phospholipid distribution revealed by freeze-fracture replica labeling. J. Cell Sci. *109*, 2453–2460.

Fujimoto, T. (1996). GPI-anchored proteins, glycosphingolipids, and sphingomyelin are sequestered to caveolae only after crosslinking. J. Histochem. Cytochem. *44*, 929–941.

Fujimoto, T., and Fujimoto, K. (1997). Metal sandwich method to quick-freeze monolayer cultured cells for freeze-fracture. J. Histochem. Cytochem. *45*, 595–598.

Furuchi, T., and Anderson, R. G. (1998). Cholesterol depletion of caveolae causes hyperactivation of extracellular signal-related kinase (ERK). J. Biol. Chem. *273*, 21099–21104.

Gaus, K., Gratton, E., Kable, E. P., Jones, A. S., Gelissen, I., Kritharides, L., and Jessup, W. (2003). Visualizing lipid structure and raft domains in living cells with two-photon microscopy. Proc. Natl. Acad. Sci. USA *100*, 15554–15559.

Gomez-Mouton, C., Abad, J. L., Mira, E., Lacalle, R. A., Gallardo, E., Jimenez-Baranda, S., Illa, I., Bernad, A., Manes, S., and Martinez, A. C. (2001). Segregation of leading-edge and uropod components into specific lipid rafts during T cell polarization. Proc. Natl. Acad. Sci. USA *98*, 9642–9647.

Gousset, K., Wolkers, W. F., Tsvetkova, N. M., Oliver, A. E., Field, C. L., Walker, N. J., Crowe, J. H., and Tablin, F. (2002). Evidence for a physiological role for membrane rafts in human platelets. J. Cell. Physiol. *190*, 117–128.

Hagiwara, A., Fukazawa, Y., Deguchi-Tawarada, M., Ohtsuka, T., and Shigemoto, R. (2005). Differential distribution of release-related proteins in the hippocampal CA3 area as revealed by freeze-fracture replica labeling. J. Comp. Neurol. *489*, 195–216.

Hakomori Si, S. I. (2002). Inaugural article: the glycosynapse. Proc. Natl. Acad. Sci. USA *99*, 225–232.

Heerklotz, H. (2002). Triton promotes domain formation in lipid raft mixtures. Biophys. J. *83*, 2693–2701.

Heider, J. G., and Boyett, R. L. (1978). The picomole determination of free and total cholesterol in cells in culture. J. Lipid Res. *19*, 514–518.

Heuser, J. E., Reese, T. S., Dennis, M. J., Jan, Y., Jan, L., and Evans, L. (1979). Synaptic vesicle exocytosis captured by quick freezing and correlated with quantal transmitter release. J. Cell Biol. *81*, 275–300.

Iwabuchi, K., Handa, K., and Hakomori, S. (1998). Separation of "glycosphingolipid signaling domain" from caveolin-containing membrane fraction in mouse melanoma B16 cells and its role in cell adhesion coupled with signaling. J. Biol. Chem. *273*, 33766–33773.

Jost, P., Brooks, U. J., and Griffith, O. H. (1973). Fluidity of phospholipid bilayers and membranes after exposure to osmium tetroxide and gluteraldehyde. J. Mol. Biol. *76*, 313–318.

Kabouridis, P. S., Janzen, J., Magee, A. L., and Ley, S. C. (2000). Cholesterol depletion disrupts lipid rafts and modulates the activity of multiple signaling pathways in T lymphocytes. Eur. J. Immunol. *30*, 954–963.

Kenworthy, A. K., Nichols, B. J., Remmert, C. L., Hendrix, G. M., Kumar, M., Zimmerberg, J., and Lippincott-Schwartz, J. (2004). Dynamics of putative raft-associated proteins at the cell surface. J. Cell Biol. *165*, 735–746.

Kenworthy, A. K., Petranova, N., and Edidin, M. (2000). High-resolution FRET microscopy of cholera toxin B-subunit and GPI-anchored proteins in cell plasma membranes. Mol. Biol. Cell *11*, 1645–1655.

Kiyokawa, E., Baba, T., Otsuka, N., Makino, A., Ohno, S., and Kobayashi, T. (2005). Spatial and functional heterogeneity of sphingolipid-rich membrane domains. J. Biol. Chem. *280*, 24072–24084.

Korlach, J., Schwille, P., Webb, W. W., and Feigenson, G. W. (1999). Characterization of lipid bilayer phases by confocal microscopy and fluorescence correlation spectroscopy. Proc. Natl. Acad. Sci. USA *96*, 8461–8466.

Kusumi, A., Koyama-Honda, I., and Suzuki, K. (2004). Molecular dynamics and interactions for creation of stimulation-induced stabilized rafts from small unstable steady-state rafts. Traffic *5*, 213–230.

Kusumi, A., and Suzuki, K. (2005). Toward understanding the dynamics of membrane-raft-based molecular interactions. Biochim. Biophys. Acta *1746*, 234–251.

Kusunoki, S., Shimizu, J., Chiba, A., Ugawa, Y., Hitoshi, S., and Kanazawa, I. (1996). Experimental sensory neuropathy induced by sensitization with ganglioside GD1b. Ann. Neurol. *39*, 424–431.

Kwik, J., Boyle, S., Fooksman, D., Margolis, L., Sheetz, M. P., and Edidin, M. (2003). Membrane cholesterol, lateral mobility, and the phosphatidylinositol 4,5-bisphosphate-dependent organization of cell actin. Proc. Natl. Acad. Sci. USA *100*, 13964–13969.

Lannert, H., Gorgas, K., Meissner, I., Wieland, F. T., and Jeckel, D. (1998). Functional organization of the Golgi apparatus in glycosphingolipid biosynthesis. Lactosylceramide and subsequent glycosphingolipids are formed in the lumen of the late Golgi. J. Biol. Chem. *273*, 2939–2946.

Magee, A. I., Adler, J., and Parmryd, I. (2005). Cold-induced coalescence of T-cell plasma membrane microdomains activates signalling pathways. J. Cell Sci. *118*, 3141–3151.

Marwali, M. R., Rey-Ladino, J., Dreolini, L., Shaw, D., and Takei, F. (2003). Membrane cholesterol regulates LFA-1 function and lipid raft heterogeneity. Blood *102*, 215–222.

Mayor, S., and Rao, M. (2004). Rafts: scale-dependent, active lipid organization at the cell surface. Traffic *5*, 231–240.

Mayor, S., Rothberg, K. G., and Maxfield, F. R. (1994). Sequestration of GPI-anchored proteins in caveolae triggered by cross-linking. Science *264*, 1948–1951.

Meder, D., Moreno, M. J., Verkade, P., Vaz, W. L., and Simons, K. (2006). Phase coexistence and connectivity in the apical membrane of polarized epithelial cells. Proc. Natl. Acad. Sci. USA *103*, 329–334.

Mukherjee, S., and Maxfield, F. R. (2004). Membrane domains. Annu. Rev. Cell Dev. Biol. *20*, 839–866.

Munro, S. (2003). Lipid rafts: elusive or illusive? Cell *115*, 377–388.

Nagatsuka, Y. *et al.* (2003). Carbohydrate-dependent signaling from the phosphatidylglucoside-based microdomain induces granulocytic differentiation of HL60 cells. Proc. Natl. Acad. Sci. USA *100*, 7454–7459.

Nam, K. S., Igarashi, K., Umeda, M., and Inoue, K. (1990). Production and characterization of monoclonal antibodies that specifically bind to phosphatidylcholine. Biochim. Biophys. Acta *1046*, 89–96.

Nichols, B. J. (2003). GM1-containing lipid rafts are depleted within clathrin-coated pits. Curr. Biol. *13*, 686–690.

Parton, R. G. (1994). Ultrastructural localization of gangliosides; GM1 is concentrated in caveolae. J. Histochem. Cytochem. *42*, 155–166.

Plowman, S. J., Muncke, C., Parton, R. G., and Hancock, J. F. (2005). H-ras, K-ras, and inner plasma membrane raft proteins operate in nanoclusters with differential dependence on the actin cytoskeleton. Proc. Natl. Acad. Sci. USA *102*, 15500–15505.

Pralle, A., Keller, P., Florin, E. L., Simons, K., and Horber, J. K. (2000). Sphingolipid-cholesterol rafts diffuse as small entities in the plasma membrane of mammalian cells. J. Cell Biol. *148*, 997–1008.

Prior, I. A., Muncke, C., Parton, R. G., and Hancock, J. F. (2003). Direct visualization of Ras proteins in spatially distinct cell surface microdomains. J. Cell Biol. *160*, 165–170.

Ripley, B. D. (1977). Modeling spatial patterns. J. R. Stat. Soc. Ser. B *39*, 172–212.

Ripley, B. D. (1979). Tests of randomness for spatial point patterns. J. R. Stat. Soc. Ser. B *41*, 368–374.

Ritchie, K., Iino, R., Fujiwara, T., Murase, K., and Kusumi, A. (2003). The fence and picket structure of the plasma membrane of live cells as revealed by single molecule techniques. Mol. Membr. Biol. *20*, 13–18.

Schnitzer, J. E., McIntosh, D. P., Dvorak, A. M., Liu, J., and Oh, P. (1995). Separation of caveolae from associated microdomains of GPI-anchored proteins. Science *269*, 1435–1439.

Schwarzmann, G., Hoffmann-Bleihauer, P., Schubert, J., Sandhoff, K., and Marsh, D. (1983). Incorporation of ganglioside analogues into fibroblast cell membranes. A spin-label study. Biochemistry *22*, 5041–5048.

Sharma, P., Varma, R., Sarasij, R. C., Ira, Gousset, K., Krishnamoorthy, G., Rao, M., and Mayor, S. (2004). Nanoscale organization of multiple GPI-anchored proteins in living cell membranes. Cell *116*, 577–589.

Simons, K., and Ikonen, E. (1997). Functional rafts in cell membranes. Nature *387*, 569–572.

Simons, M., Friedrichson, T., Schulz, J. B., Pitto, M., Masserini, M., and Kurzchalia, T. V. (1999). Exogenous administration of gangliosides displaces GPI-anchored proteins from lipid microdomains in living cells. Mol. Biol. Cell *10*, 3187–3196.

Sonnino, S., and Chigorno, V. (2000). Ganglioside molecular species containing C18- and C20-sphingosine in mammalian nervous tissues and neuronal cell cultures. Biochim. Biophys. Acta *1469*, 63–77.

Takamiya, K. *et al.* (1996). Mice with disrupted GM2/GD2 synthase gene lack complex gangliosides but exhibit only subtle defects in their nervous system. Proc. Natl. Acad. Sci. USA *93*, 10662–10667.

Taki, T., and Ishikawa, D. (1997). TLC blotting: application to microscale analysis of lipids and as a new approach to lipid-protein interaction. Anal. Biochem. *251*, 135–143.

Thompson, T. E., Allietta, M., Brown, R. E., Johnson, M. L., and Tillack, T. W. (1985). Organization of ganglioside GM1 in phosphatidylcholine bilayers. Biochim. Biophys. Acta *817*, 229–237.

Varma, R., and Mayor, S. (1998). GPI-anchored proteins are organized in submicron domains at the cell surface. Nature *394*, 798–801.

Vie, V., Van Mau, N., Lesniewska, E., Goudonnet, J. P., Heitz, F., and Le Grimelle, C. (1998). Distribution of ganglioside GM1 between two-component, two-phase phosphatidylcholine monolayers. Langmuir *14*, 4754–4783.

Wang, T. Y., and Silvius, J. R. (2003). Sphingolipid partitioning into ordered domains in cholesterol-free and cholesterol-containing lipid bilayers. Biophys. J. *84*, 367–378.

Williams, M. A., and McCluer, R. H. (1980). The use of Sep-Pak C18 cartridges during the isolation of gangliosides. J. Neurochem. *35*, 266–269.

Yuan, C., Furlong, J., Burgos, P., and Johnston, L. J. (2002). The size of lipid rafts: an atomic force microscopy study of ganglioside GM1 domains in sphingomyelin/DOPC/cholesterol membranes. Biophys. J. *82*, 2526–2535.

Yuan, C., and Johnston, L. J. (2000). Distribution of ganglioside GM1 in L-alpha-dipalmitoylphosphatidylcholine/cholesterol monolayers: a model for lipid rafts. Biophys. J. *79*, 2768–2781.

Zhou, X., and Arthur, G. (1992). Improved procedures for the determination of lipid phosphorus by malachite green. J. Lipid Res. *33*, 1233–1236.

www.nature.com/clinicalpractice/neuro

Predictors of respiratory failure in Guillain–Barré syndrome

Original article Durand MC *et al.* (2006) Clinical and electrophysiological predictors of respiratory failure in Guillain–Barré syndrome: a prospective study. *Lancet Neurol* 5: 1021–1028

SYNOPSIS

KEYWORDS electrophysiological testing, Guillain–Barré syndrome, mechanical ventilation, prognosis, vital capacity

BACKGROUND

In patients with Guillain–Barré syndrome (GBS), respiratory failure—the most serious short-term complication of the condition—can be difficult to anticipate.

OBJECTIVE

To identify clinical and electrophysiological predictors of respiratory failure in patients with GBS.

DESIGN AND INTERVENTION

The investigators prospectively collected data on 154 adults with idiopathic GBS who had not previously received ventilatory support and who were referred to a French hospital between September 1998 and January 2006. At study inclusion, a single neurophysiologist recorded the compound muscle action potential (CMAP) after distal and proximal stimulation, the conduction velocity, the distal latency and the F-wave latency in the median, ulnar and common peroneal nerves. The electrophysiological patterns were classified as demyelinating, axonal, unexcitable, equivocal or normal. Disability grade, arm grade, inability to lift the head and vital capacity were also assessed. Mechanical ventilation was initiated at the discretion of the treating physician, who was unaware of the electrophysiological details. The investigators used Classification and Regression Tree (CART) analysis to identify the factors that best predicted the requirement for mechanical ventilation in 103 patients (model-fitting set), with the following factors included in the analysis: electrophysiological data, vital capacity, delay between GBS onset and admission, and inability to lift the head. The selected decision tree model was validated in 51 patients (validation set) who were matched with the model-fitting set for the prevalence of mechanical ventilation.

OUTCOME MEASURE

The main outcome of the study was the ability of the model selected by CART analysis to predict respiratory failure in patients with GBS.

RESULTS

Thirty-four patients required ventilation after inclusion in the study. At baseline, these patients had more limb weakness (worse disability and arm grades; $P<0.0001$ and $P=0.002$, respectively), greater inability to lift the head ($P=0.02$), greater respiratory muscle weakness (lower values for vital capacity; $P<0.0001$), higher rates of bulbar and liver dysfunction ($P<0.0001$ and $P=0.02$, respectively) and higher rates of demyelinating electrophysiology ($P=0.003$) than did patients who did not require ventilation. The optimum decision tree model retained vital capacity and extent of conduction block (proximal/distal CMAP amplitude ratio) of the common peroneal nerve as predictive factors. In the model-fitting set, individuals with a proximal/distal CMAP amplitude ratio of at least 0.556 and a vital capacity below 80% had a 16-fold increased risk of requiring mechanical ventilation compared with patients who had a proximal/distal CMAP amplitude ratio of at least 0.556 and a vital capacity above 80% (odds ratio 16.1, 95% CI 1.9–132; $P=0.001$); the risk was increased 41-fold in patients with a proximal/distal CMAP amplitude ratio below 0.556 (odds ratio 41.0, 95% CI 4.8–353; $P=0.0007$). Comparable results were obtained for the validation set.

CONCLUSION

Vital capacity and the proximal/distal CMAP amplitude ratio of the common peroneal nerve are useful predictors of respiratory failure in patients with GBS.

www.nature.com/clinicalpractice/neuro

COMMENTARY

Susumu Kusunoki* and Pieter van Doorn

GBS is an acute monophasic autoimmune neuropathy that is usually preceded by an infection. Although intravenous immunoglobulin therapy and plasma exchange hasten recovery and improve long-term outcome, about 20% of patients need artificial ventilation, 20% remain unable to walk after half a year, and 5% die. GBS is, therefore, still a devastating and potentially life-threatening disease. Accurate prediction of the disease course is important for optimum treatment, and might improve outcome.

Several clinical factors, such as age, presence of diarrhea and severity of muscle weakness early in the disease course, are known to be associated with the prognosis of GBS. In the present study, Durand *et al.* found that patients with evidence of demyelination were at increased risk of requiring mechanical ventilation. Their results also indicate that the proximal/distal CMAP amplitude ratio of the common peroneal nerve might be reflective of overall disease burden in GBS. Along with vital capacity, this ratio can predict respiratory failure and prognosis in GBS.

It is unclear why demyelination is associated with respiratory failure, whereas axonal degeneration is not. In North America and Europe, most patients with GBS have acute inflammatory demyelinating polyneuropathy (AIDP). For example, in one report from Europe, 69% of patients with GBS had AIDP, only 3% had acute motor axonal neuropathy (AMAN), and 23% had equivocal electrophysiology.[1] Patients with AIDP (definite evidence of demyelination) might have more-severe clinical manifestations than do patients with equivocal electrophysiology (no definite evidence of demyelination), resulting in an increased requirement for artificial ventilation among patients with demyelinating GBS. Demyelination itself, however, is not necessarily a factor that is specifically associated with the pathogenesis of respiratory failure—in the current study, 51% of patients who did not require ventilation also had electrophysiological evidence of demyelination. In addition, it should be pointed out that initial demyelinating electrophysiology does not preclude the subsequent development of axonal injury, which might be associated with a poor prognosis at 6 months.

In this context, we should also consider the variation in GBS type among different genetic or geographical populations. For example, AMAN has been reported to be more frequent in China and Japan than in Western countries.[2] Among Japanese patients, the prevalence of AIDP was similar among ventilated and nonventilated patients.[3] The predictive factors for artificial ventilation might, therefore, be different for Asian patients with GBS.

The presence of antiganglioside antibodies is another possible predictor of respiratory failure in GBS. In Japanese patients with GBS, anti-GQ1b IgG antibodies are more frequently detected in ventilated than in nonventilated patients[3]—a difference not found by Durand *et al.* Again, a variation in genetic background might contribute to the difference. The frequency of bulbar dysfunction, which is associated with the presence of anti-GQ1b and anti-GT1a antibodies,[4] is, however, significantly increased in ventilated patients with GBS both in Japan[3] and in Western countries. Differences in the antibody assays used might partly explain these conflicting observations. Recently, anti-GD1a–GD1b complex and anti-GD1b–GT1b complex IgG antibodies have also been reported to be predictors of the need for artificial ventilation.[2]

In conclusion, the identification of readily available clinical or electrophysiological data that can predict the requirement for artificial ventilation in patients with GBS is an important development. It seems that the presence of specific antiganglioside antibodies and a patient's genetic or geographical background also have prognostic relevance in GBS. Further studies are needed to elucidate the pathogenetic mechanisms involved in the development of respiratory failure in GBS.

References

1 Hadden RDM *et al.* (1998) Electrophysiological classification of Guillain-Barré syndrome: clinical associations and outcome. *Ann Neurol* **44:** 780–788
2 Kaida K *et al.* (2007) Anti-ganglioside complex antibodies associated with severe disability in GBS. *J Neuroimmunol* **182:** 212–218
3 Kaida K *et al.* (2004) Anti-GQ1b antibody as a factor predictive of mechanical ventilation in Guillain-Barré syndrome. *Neurology* **62:** 821–824
4 O'Leary CP *et al.* (1996) Acute oropharyngeal palsy is associated with antibodies to GQ1b and GT1a gangliosides. *J Neurol Neurosurg Psychiatry* **61:** 649–651

S Kusunoki is Professor and Chairman of the Department of Neurology, Kinki University School of Medicine, Osaka, Japan, and P van Doorn is Professor of neuromuscular disorders at the Department of Neurology, Erasmus Medical Center in Rotterdam, The Netherlands.

Acknowledgments
The synopsis was written by Martina Habeck, Associate Editor, Nature Clinical Practice.

Competing interests
The authors declared they have no competing interests.

Correspondence
*Department of Neurology
Kinki University School of Medicine
377-2 Ohno-Higashi
Osaka-Sayama
Osaka 589-8511
Japan
kusunoki-tky@umin.ac.jp

Received 5 February 2007
Accepted 9 May 2007
Published online
19 June 2007
www.nature.com/clinicalpractice
doi:10.1038/ncpneuro0535

PRACTICE POINT
When determining the risk of respiratory failure in GBS, vital capacity and the extent of conduction block of the common peroneal nerve seem to be useful predictive markers, but clinical and genetic factors should also be taken into account

Available online at www.sciencedirect.com
ScienceDirect
Experimental Neurology 209 (2008) 279–283
Experimental Neurology
www.elsevier.com/locate/yexnr

Short Communication

Apoptosis of primary sensory neurons in GD1b-induced sensory ataxic neuropathy

Kazuo Takada [a], Jun Shimizu [b], Susumu Kusunoki [a,*]

[a] Department of Neurology, Kinki University School of Medicine, 377-2 Ohno-Higashi, Osaka-Sayama, Osaka 589-8511, Japan
[b] Department of Neurology, Graduate School of Medicine, University of Tokyo, 7-3-1 Hongo, Bunkyo-ku, Tokyo 113-8655, Japan

Received 22 May 2007; revised 4 September 2007; accepted 10 September 2007
Available online 21 September 2007

Abstract

Experimental autoimmune sensory ataxic neuropathy was induced in three of six rabbits sensitized with GD1b ganglioside (GD1b-SAN). TUNEL assay was performed on sections of dorsal root ganglia in the cauda equina. The results showed the presence of TUNEL-positive neurons in all three rabbits affected with GD1b-SAN. In contrast, no such neurons were observed in any of the sections from the unaffected rabbits that had been inoculated with GD1b, rabbits inoculated with adjuvant alone or those without inoculation. These data support that an apoptotic mechanism is involved in the pathogenesis of GD1b-SAN.

Keywords: Ganglioside; Neuropathy; Guillain–Barré syndrome; Autoimmunity; Antibody; Apoptosis; Sensory neuron; Dorsal root ganglion

Introduction

Antiganglioside antibodies are frequently present in sera from patients with autoimmune neuropathies, such as Guillain–Barré syndrome and IgM paraproteinemic neuropathy (Kusunoki, 2000; Willison and Yuki, 2002). Immunohistochemical studies have demonstrated that some gangliosides exhibit a unique localization in the nervous system (Kusunoki et al., 1993; Chiba et al., 1993; Kaida et al., 2003). The antibodies to these gangliosides may therefore be associated with unique clinical features by binding to regions in which the target antigen gangliosides are localized.

Immunohistochemistry using a monoclonal antibody against GD1b ganglioside has shown that GD1b is densely localized in the large neurons in the dorsal root ganglia (DRGs) of rabbits as well as humans (Kusunoki et al., 1993, 1996). These large neurons are known to mediate proprioception. IgM M-proteins that recognize a disialosyl residue of GD1b are specifically present in sera from patients with sensory ataxic neuropathy (Willison et al., 2001). We have previously reported that sensitization of rabbits with GD1b induces sensory ataxic neuropathy (GD1b-SAN) (Kusunoki et al., 1996), in which IgG antibodies monospecific to GD1b is essential to the pathogenesis of the disease (Kusunoki et al., 1999a). GD1b-SAN is the first established animal model of autoimmune neuropathy mediated by antiganglioside antibodies. Passive transfer of anti-GD1b antisera from rabbits affected with GD1b-SAN-induced degeneration of rabbit sensory neurons, indicating that anti-GD1b antibody is directly involved in the pathogenesis of GD1b-SAN (Kusunoki et al., 1999b). The precise mechanism by which the anti-GD1b antibody causes the disease remains to be elucidated.

Pathological investigation of GD1b-SAN demonstrated that there was no lymphocytic infiltration in the affected regions. Degeneration of the axons was evident in the dorsal root and dorsal column with macrophage infiltration (Kusunoki et al., 1996). In contrast, in spite of the looseness of the blood–nerve barrier in the DRG, there was no significant finding in the DRG except for few Nageotte nodules (Kusunoki et al., 1996). This prompted us to investigate the possibility that the anti-GD1b antibody induces apoptosis of the large sensory neurons.

* Corresponding author. Fax: +81 72 368 4846.
E-mail address: kusunoki-tky@umin.ac.jp (S. Kusunoki).

0014-4886/$ - see front matter © 2007 Elsevier Inc. All rights reserved.
doi:10.1016/j.expneurol.2007.09.010

Through the use of terminal deoxynucleotidyl tranferase (TdT)-mediated dUTP-biotin nick end-labeling (TUNEL) assay, we found evidence of apoptosis in the DRGs from GD1b-SAN-affected rabbits.

Materials and methods

Immunization with GD1b was performed as described previously (Kusunoki et al., 1996). Six rabbits were immunized

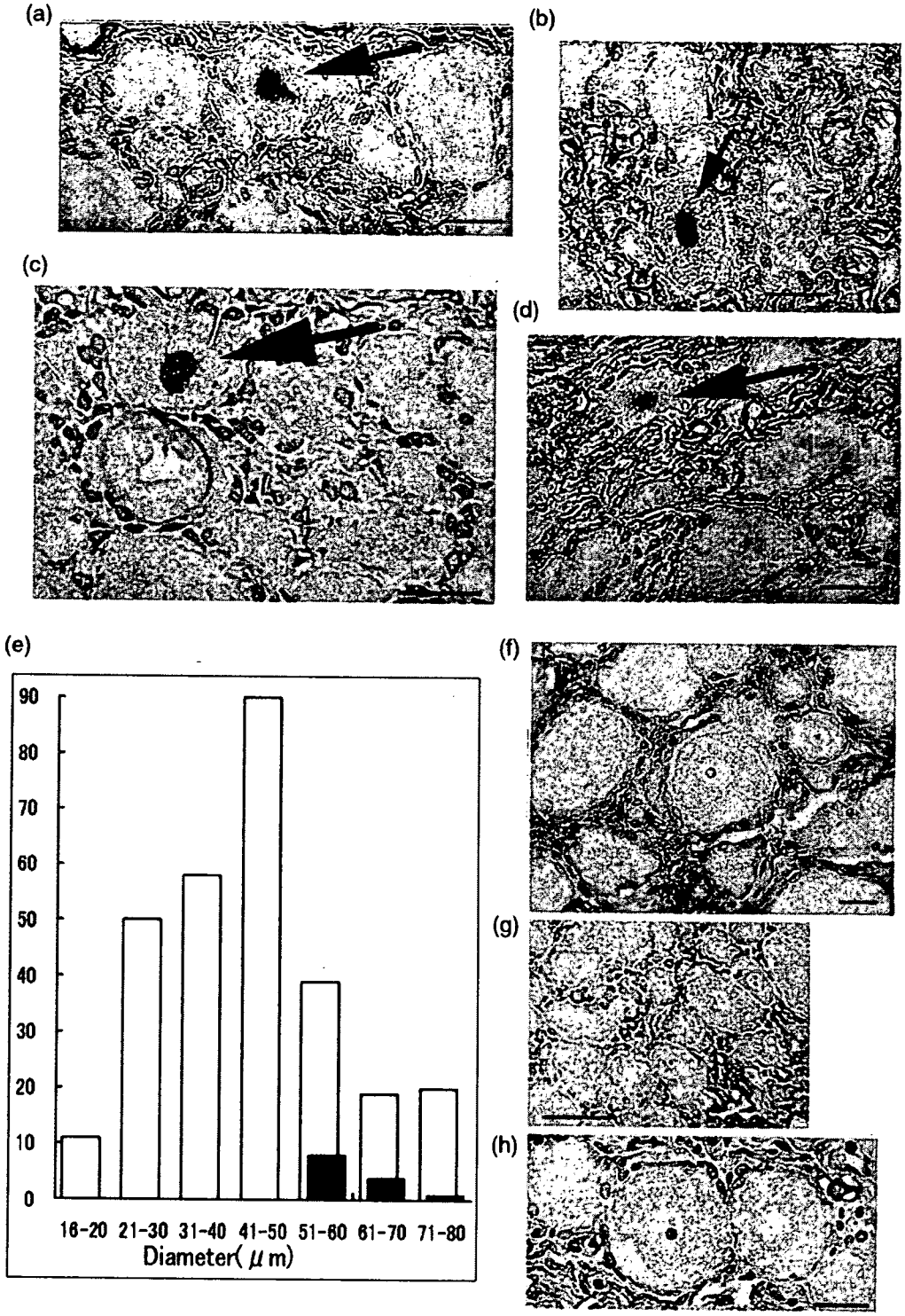

Fig. 1. (a–d) TUNEL assay of sections from rabbits affected with GD1b-SAN. Primary sensory neurons containing nucleotides that react positively (arrows). Scale bar=50 μm. (e) The histogram of the diameters of TUNEL-positive and TUNEL-negative neurons. The TUNEL-positive neurons were of large ones. (f–h) TUNEL assay of sections from unaffected rabbits inoculated with GD1b (f), inoculated with adjuvant alone (g) and without any inoculation (h). No TUNEL-positive cells were observed. Scale bar=50 μm.

with GD1b, and two were given the same inoculum without GD1b. Two rabbits without inoculation were also kept in the same room of the animal center. Serum samples were taken by ear vein puncture at 1- or 2-week intervals. The rabbits were checked daily for clinical signs and weighed twice per week.

Serum anti-GD1b antibodies were investigated by the use of enzyme-linked immunosorbent assay, as described previously (Kusunoki et al., 1996). Microtiter wells were coated with 200 ng of GD1b, with an uncoated well serving as the control. Peroxidase-conjugated antibody to rabbit IgM (mu-chain specific; Cappel, West Chester, PA; diluted 1:400) or rabbit IgG (gamma-chain specific; Southern Biotechnology Associates Inc., Birmingham, USA; diluted 1:2000) was used as the secondary antibody. The optical density (OD; 492 nm) was corrected by subtracting the OD of the control well that had been processed in the same manner. A reaction with a corrected OD of more than 0.1 was considered positive.

The rabbits affected with GD1b-SAN were sacrificed 2 or 3 days after the neurological onset (namely, 35, 42 and 90 days after the first inoculation, respectively). The rabbits that had been immunized with GD1b but did not exhibit any neurological problems were sacrificed 121, 136 and 156 days after the first inoculation. The rabbits inoculated with adjuvant alone were sacrificed on day 35 and 42 after the first inoculation and those without any inoculation were sacrificed after 14 and 21 days of observation.

The lumbar spinal cord and the DRGs in the cauda equina were removed from all of the rabbits except for the two unaffected GD1b-sensitized rabbits (sacrificed on 121 and 136 days after first inoculation). Specimens were fixed either in 4% formaldehyde in phosphate-buffered saline for 48 h or in 2.5% glutaraldehyde and 2% paraformaldehyde buffered with 0.1 M sodium cacodylate (half Karnovsky solution) for 12 h.

The formaldehyde-fixed specimens were embedded in paraffin and serial sections, 10 μm in thickness, were prepared. TUNEL assay was performed using a kit (Wako Pure Chemical Industries, Osaka, Japan) according to the manufacturer's instructions. Briefly, the sections underwent protein digestion at 37 °C for 5 min, after deparaffinization and hydration. After washing, they were incubated with 50 μl of TdT reaction solution for 10 min in a moist chamber at 37 °C. After inactivation of intrinsic peroxidase, sections were incubated with 100 μl of peroxidase-conjugated antibody solution for 10 min in a moist chamber at 37 °C. After removing the antibody solutions, they were incubated with 100 μl of diaminobenzidine solution for 5 min at room temperature. After washing, sections were dehydrated and covered with a cover glass. The sections of DRGs in the cauda equina obtained from each of the three rabbits affected with GD1b-SAN, each of the two adjuvant controls, one unaffected rabbit sensitized with GD1b, and two rabbits without inoculation were examined with TUNEL assay. Seventy sections from each rabbit were examined. In the DRGs from the affected rabbits, the diameters of the TUNEL-positive and TUNEL-negative neurons containing a nucleus were measured. Immunohistochemistry with anti-caspase 3 antibody also was performed on deparaffinized sections as described by Gown and Willingham (Gown and Willingham, 2002). Mouse monoclonal anti-caspase 3 (3G2, 1:40 diluted, Abcam, Cambridge, UK) was used as the primary antibody, and peroxidase-conjugated goat

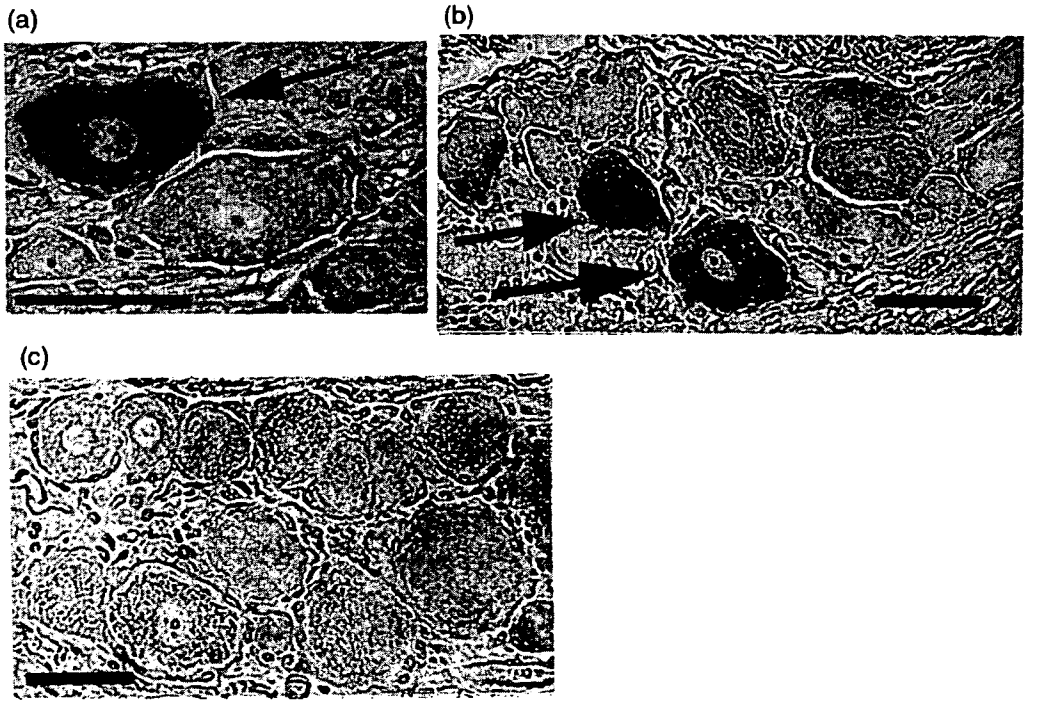

Fig. 2. Immunohistochemistry using anti-caspase 3 antibody. (a and b) Some DRG neurons from rabbits affected with GD1b-SAN were immunostained with anti-caspase 3 antibody (arrows). (c) No such staining was observed in DRG from a rabbit inoculated with adjuvant alone. Scale bar=50 μm.

anti-mouse IgG (1:250 diluted, MP Biomedicals, Ohio, USA) was the secondary antibody.

The Karnovsky-fixed specimens were postfixed in 2% osmium tetroxide for 2 h, dehydrated with ethanol and embedded in epoxy resin. Semi-thin sections, 1.0 μm in thickness, were cut from the Epon block and were stained with toluidine blue.

The experiments involving animals were approved by the local ethics committee in Kinki University.

Results

Anti-GD1b IgM antibody was detected 2 weeks after the first inoculation and reached a maximum at 4 weeks. IgG anti-GD1b antibody was elevated later, after the elevation of IgM.

Three of the six rabbits immunized with GD1b developed SAN 33, 40 and 88 days after the first inoculation, respectively.

In the sections stained with toluidine blue, axonal degeneration of the dorsal column of the spinal cord was evident, as described previously.

A few TUNEL-positive cells were observed in the formaldehyde-fixed sections from all three rabbits affected with GD1b-induced SAN (Figs. 1a–d). Two sections were mounted on each glass slide, in which approximately one TUNEL-positive cell was observed. In contrast, no TUNEL-positive cells were observed in any section from the unaffected rabbits that had been immunized with GD1b (Fig. 1f), the rabbits inoculated with adjuvant alone (Fig. 1g) or the rabbits without inoculation (Fig. 1h).

Of the 300 neurons of DRGs from the affected rabbits, 13 were TUNEL-positive and 287 were TUNEL-negative. The histogram was shown in Fig. 1e.

A few neurons per section of DRG from the affected rabbits were immunostained with anti-caspase 3 antibody, whereas no such staining was seen in DRG from control rabbits (Fig. 2).

Discussion

Anti-GD1b antibodies were detected in all six rabbits sensitized with GD1b. Three of those six rabbits developed SAN. This finding is compatible with the previous results that about half of the rabbits sensitized with GD1b developed SAN (Kusunoki et al., 1996, 1999a).

We previously reported that downregulation of trkC occurs in the dorsal root ganglia from rabbits in the acute phase of GD1b-SAN (Hitoshi et al., 1999). TrkC serves as a receptor for neurotrophin-3 (NT3). It is known that the large primary sensory neurons in the dorsal root ganglia, which mediate proprioception, depend mainly on neurotrophin-3-mediated trkC signaling. It has been reported that mice defective for trkC exhibit abnormal movement due to lack of proprioception (Klein et al., 1994). Our above result of trkC downregulation therefore suggests that anti-GD1b antibody-mediated trkC downregulation and subsequent apoptosis of the large neurons of DRG contribute to the pathogenesis of GD1b-SAN.

The present investigation provides clear evidence that an apoptotic mechanism is involved in the pathogenesis of GD1b-SAN. Positive immunostaining of some DRG neurons from affected rabbits with anti-caspase 3 antibody also indicates the involvement of an apoptotic mechanism in GD1b-SAN. Although the number of neurons with apoptotic changes appears to be small, approximately 4% of neurons were TUNEL-positive, indicating that quite a few sensory neurons could be affected in each animal. An apoptotic neuron should not remain *in situ* for a long time but would soon disappear. Therefore, we were not able to identify many apoptotic neurons at the same time in the pathological specimens.

Gangliosides are known to form microdomains called lipid rafts (Simons and Toomre, 2000). Within the rafts, gangliosides are believed to interact with important transmembrane receptors or signal transducers (Kasahara et al., 2000). Treatment of rat cerebellar cultures with a monoclonal anti-ganglioside GD3 antibody induced the activation of the Src family kinase Lyn and rapid tyrosine phosphorylation of some proteins (Kasahara et al., 1997). Thus, antiganglioside antibodies may alter the function of neurons through binding to target gangliosides in the raft. The mechanism(s) by which antibody binding causes apoptosis and whether the downregulation of trkC is involved in the process need to be clarified in future investigations.

Neuropathy with IgM M-protein binding to a disialosyl residue of several gangliosides, including GD1b, GT1b and GQ1b, is a human counterpart of GD1b-SAN (Willison et al., 2001). There has been one reported autopsy case of this kind of neuropathy, demonstrating a reduction in the number of sensory neurons in the DRG and pallor of the dorsal column in the spinal cord (Obi et al., 1999). In addition to the IgM paraproteinemic neuropathy, GBS with a monospecific anti-GD1b IgG antibody has been associated with ataxia due to disturbance in deep sensation (Wicklein et al., 1997). It has been reported that human IgM monoclonal antibody recognizing GD2, GD1b, GT1b and GQ1b resulted in death of rat dorsal root ganglion neurons (Ohsawa et al., 1993). However, the precise mechanism was not elucidated. Our present findings strongly suggest that apoptosis of the large primary sensory neurons contributes to the pathogenesis of human neuropathies with antibodies recognizing gangliosides with disialosyl residue, in particular GD1b.

Acknowledgments

This work was supported in part by Grants-in Aid for Scientific Research (18390264) from the Ministry of Education, Culture, Sports, Science and Technology of Japan, and by a Health Sciences Research Grant on Psychiatric and Neurological Diseases and Mental Health and a Research Grant for Neuroimmunological Diseases from the Ministry of Health, Labour and Welfare of Japan.

References

Chiba, A., Kusunoki, S., Obata, H., Machinami, R., Kanazawa, I., 1993. Serum anti-GQ1b IgG antibody is associated with ophthalmoplegia in Miller Fisher syndrome and Guillain–Barre syndrome: clinical and immunohistochemical studies. Neurology 43, 1911–1917.

Gown, A.M., Willingham, M.C., 2002. Improved detection of apoptotic cells in archival paraffin sections: immunohistochemistry using antibodies to cleaved caspase 3. J. Histochem. Cytochem. 50, 449–454.

Hitoshi, S., Kusunoki, S., Murayama, S., Tsuji, S., Kanazawa, I., 1999. Rabbit experimental sensory ataxic neuropathy: anti-GD1b antibody-mediated trkC downregulation of dorsal root ganglia neurons. Neurosci. Lett. 260, 157–160.

Kaida, K., Kusunoki, S., Kamakura, K., Motoyoshi, K., Kanazawa, I., 2003. GalNAc-GD1a in human peripheral nerve: target sites of anti-ganglioside antibody. Neurology 61, 465–470.

Kasahara, K., Watanabe, Y., Yamamoto, T., Sanai, Y., 1997. Association of Src family tyrosine kinase Lyn with ganglioside GD3 in rat brain. Possible regulation of Lyn by glycosphingolipid in caveolae-like domains. J. Biol. Chem. 272, 29947–29953.

Kasahara, K., Watanabe, K., Takeuchi, K., Kaneko, H., Oohira, A., Yamamoto, T., Sanai, Y., 2000. Involvement of gangliosides in glycosylphosphatidylinositol-anchored neuronal cell adhesion molecule TAG-1 signaling in lipid rafts. J. Biol. Chem. 275, 34701–34709.

Klein, R., Silos-Santiago, I., Smeyne, R.J., Lira, S.A., Brambilla, R., Bryant, S., Zhang, L., Snider, W.D., Barbacid, M., 1994. Disruption of the neurotrophin-3 receptor gene trkC eliminates la muscle afferents and results in abnormal movements. Nature 368, 249–251.

Kusunoki, S., 2000. Antiglycolipid antibodies in Guillain–Barre syndrome and autoimmune neuropathies. Am. J. Med. Sci. 319, 234–239.

Kusunoki, S., Chiba, A., Tai, T., Kanazawa, I., 1993. Localization of GM1 and GD1b antigens in the human peripheral nervous system. Muscle Nerve 16, 752–756.

Kusunoki, S., Shimizu, J., Chiba, A., Ugawa, Y., Hitoshi, S., Kanazawa, I., 1996. Experimental sensory neuropathy induced by sensitization with ganglioside GD1b. Ann. Neurol. 39, 424–431.

Kusunoki, S., Hitoshi, S., Kaida, K., Murayama, S., Kanazawa, I., 1999a. Degeneration of rabbit sensory neurons induced by passive transfer of anti-GD1b antiserum. Neurosci. Lett. 273, 33–36.

Kusunoki, S., Hitoshi, S., Kaida, K., Arita, M., Kanazawa, I., 1999b. Monospecific anti-GD1b IgG is required to induce rabbit ataxic neuropathy. Ann. Neurol. 45, 400–403.

Obi, T., Murakami, T., Takatsu, M., Kusunoki, S., Serizawa, M., Mizoguchi, K., Koike, R., Nishimura, Y., 1999. Clinicopathological study of an autopsy case with sensory-dominant polyradiculoneuropathy with antiganglioside antibodies. Muscle Nerve 22, 1426–1431.

Ohsawa, T., Miyatake, T., Yuki, N., 1993. Anti-B-series ganglioside-recognizing autoantibodies in an acute sensory neuropathy patient cause cell death of rat dorsal root ganglion neurons. Neurosci. Lett. 157, 167–170.

Simons, K., Toomre, D., 2000. Lipid rafts and signal transduction. Nat. Rev., Mol. Cell Biol. 1, 31–39.

Wicklein, E.M., Pfeiffer, G., Yuki, N., Hartard, C., Kunze, K., 1997. Prominent sensory ataxia in Guillain–Barre syndrome associated with IgG anti-GD1b antibody. J. Neurol. Sci. 151, 227–229.

Willison, H.J., Yuki, N., 2002. Peripheral neuropathies and anti-glycolipid antibodies. Brain 125, 2591–2625.

Willison, H.J., O'Leary, C.P., Veitch, J., Blumhardt, L.D., Busby, M., Donaghy, M., Fuhr, P., Ford, H., Hahn, A., Renaud, S., Katifi, H.A., Ponsford, S., Reuber, M., Steck, A., Sutton, I., Schady, W., Thomas, P.K., Thompson, A.J., Vallat, J.M., Winer, J., 2001. The clinical and laboratory features of chronic sensory ataxic neuropathy with anti-disialosyl IgM antibodies. Brain 124, 1968–1977.